

Coherent feedforward loops can be used to approximately compute log-likelihood ratio for detecting persistent signals

Chun Tung Chou
School of Computer Science and Engineering,
University of New South Wales,
Sydney, NSW 2052, Australia
E-mail: c.t.chou@unsw.edu.au

July 29, 2022

Abstract

Living cells need to distinguish persistent signals from transient ones. There is few work on studying persistent detection, in the context of cell signalling, from a stochastic signal point of view. This paper aims to address this gap. This paper considers a persistence detection problem defined over a reaction pathway consisting of three species: an inducer, a transcription factor (TF) and a gene, where the inducer can activate the TF and an active TF can bind to the gene promoter. We model the pathway using chemical master equation so the counts of bound promoters over time is a stochastic signal. We consider the problem of using the continuous-time stochastic signal of the counts of bound promoters to infer whether the inducer signal is persistent or not. We use statistical detection theory to derive the solution to this detection problem, which is to compute the log-likelihood ratio of observing a persistent signal to a transient one. We then show that, if the input is persistent, then the positive part of the log-likelihood ratio can be approximately computed by using the continuous-time signals of the number of active TF molecules and the number of bound promoters. Finally, we show how we can use a coherent feedforward loop to approximately compute this log-likelihood ratio.

Keywords:

Systems biology; coherent feedforward loops; detection of persistent signals; detection theory; likelihood ratio; biological computation; time-scale separation.

1 Introduction

Cells live in a noisy environment. A task that cells need to do is to distinguish a persistent signal from a spurious one. Let us take the bacteria *Escherichia coli* (*E. coli*) as an example. *E. coli* can metabolise a few different types of sugar [2]. For each type of sugar, *E. coli* need to produce a specific enzyme in order to digest it. One of the prerequisites for producing an enzyme is that the specific sugar digested by the enzyme must be present in sufficient quantity for a long enough time [19]. If we consider the concentration of a sugar over time as a signal, then *E. coli* need to decide whether this signal is transient or persistent. This is an example of persistence detection that *E. coli* need to carry out.

A biochemical circuit that can perform persistence detection in *E. coli* is the L-arabinose utilisation system [19]. This circuit belongs to a general class of circuits which is known as the *Coherent Type-1 Feedforward Loop with an AND logic at the output* or C1-FFL for short. The C1-FFL is a network motif and is a frequently found circuit in both *E. coli* and *Saccharomyces cerevisiae* (yeast) [22, 26]. This means that C1-FFL carries out important functions in cells. The authors in [26, 18] show that C1-FFL can act as a persistence detector. They do this by modelling the gene expression in C1-FFL by using ordinary differential equations (ODEs) and show that a persistent (resp. transient) input to C1-FFL will result in a high (zero) output.

The papers [26, 18] take a deterministic approach to understand persistence detection. In our recent paper [7], we present a stochastic approach based on statistical detection theory [16]. In [7], we consider a reaction pathway with two species — say for concreteness, an inducer and a transcription factor (TF) — modelled by chemical master equation. We consider a detection problem whose aim is to infer whether the inducer signal is persistent or not by using the signal of the number of active TFs over time. According to detection theory, the solution to this detection problem is to compute a log-likelihood ratio and we derive an ODE which describes the evolution of this log-likelihood ratio over time. In order to connect this ODE with C1-FFL, we ask the question of how we can implement this ODE using chemical reactions. There has been a lot of work in synthetic biology on how to use chemical reactions for analog computation, see e.g. [24, 28, 29]. A lesson that we have learnt is that some computations (e.g. those involving both positive and negative numbers) are more complex to implement than others because their implementations require a higher number of chemical species and chemical reactions. This lesson leads us to derive an ODE which can approximately compute the log-likelihood ratio without having to use the computations that are complex to implement. We achieve this approximation by using time-scale separation and computing only the positive part of the log-likelihood ratio. In the final step, we show that the computation of the approximate positive log-likelihood ratio can be implemented by a C1-FFL. The paper [7] is the first to demonstrate that C1-FFL can work as a statistical persistence detector.

Although we are able to show in [7] that C1-FFL can be used as a statistical persistence detector, the C1-FFL used in [7] has a particular form where the AND gate of the C1-FFL is formed by the product of the concentration of the TF and a Hill function. However, the more common form of C1-FFL used in the literature [18, 1] has the product of two Hill

functions at the AND gate. A question is whether the more common form of C1-FFL may be related to a different persistence detection problem. In this paper, we show that this is the case.

This paper considers a reaction pathway consisting of three chemical species: an inducer, a TF and a gene. In this reaction pathway, the inducer activates the TF and the activated TF binds probabilistically with the gene promoter. We consider the detection problem of using the time signal of the number of bound promoters to infer whether the inducer signal is persistent or not. We present the solution of this detection problem in the form of an ODE which describes the evolution of the log-likelihood ratio over time. When the input is persistent, we show how we can approximately compute the log-likelihood ratio from the noisy time signals of the number of bound promoters and the number of active TFs. We then use this result to show how we can use the more common form of C1-FFL to approximately compute the positive part of the log-likelihood ratio. The key result of this paper is to show that the more common form of C1-FFL can act as a statistical detector in an inducer-TF-gene pathway. Furthermore, the methodology in this paper can be useful for designing synthetic molecular circuits for performing signal processing tasks.

If we compare this paper against our previous work [7], there are a few differences. First, the derivation in this paper is technically more involved because of the nonlinearity in the TF-gene promoter binding. Second, the form of the C1-FFL being used in this paper is different from that in [7]. This shows that there is a dependence on the form of the biochemical circuit on the associated signal processing problem. Third, this paper reveals an interesting parallel processing architecture in biochemical circuits. One of the genes in C1-FFL has two promoters. We find that one promoter is used to produce the signal for statistical persistence detection while the other promoter is used to process this signal by approximately computing log-likelihood ratio.

Note that this paper is a much expanded version of our earlier conference paper [9] which contains only the key mathematical and some numerical results. New contents of his paper include: a section on why C1-FFL can be used to approximately compute the positive part of the log-likelihood ratio, a discussion on why likelihood ratio is a suitable metric for some biological decision problems, new numerical results and all the mathematical proofs.

The rest of this paper is organised as follows. Sec. 2 presents background information on C1-FFL and detection theory. We then define the detection problem and present its solution in Sec. 3. After that in Sec. 4, we present a method to approximately compute the log-likelihood ratio and use this approximation in Sec. 5 to show that C1-FFL can be used to approximately compute the positive part of the log-likelihood ratio. Finally, Sec. 6 presents a discussion and concludes the paper.

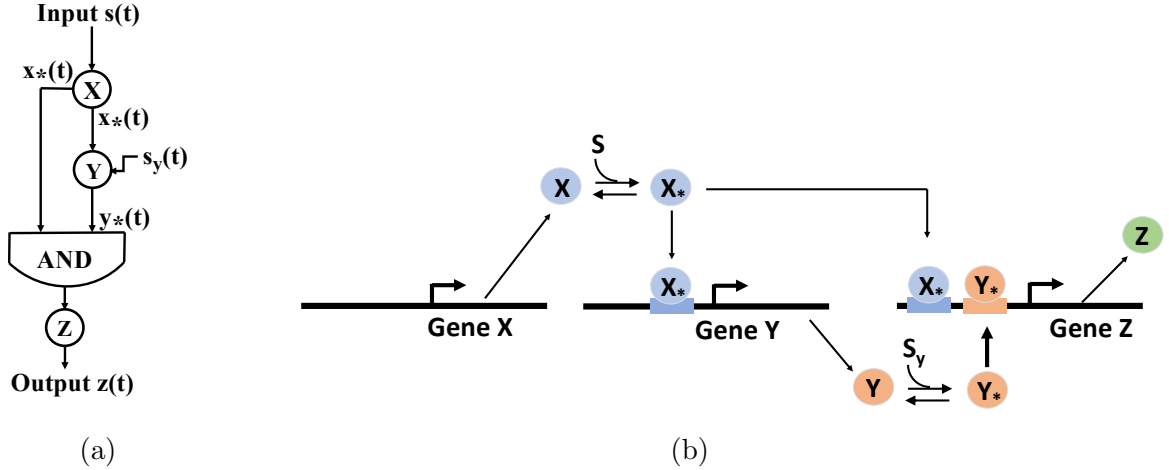


Figure 1: The coherent type-1 feedforward loop with AND logic or C1-FFL. (a) Network representation. (b) Representation with inducers, transcription factors and genes.

2 Background

2.1 C1-FFL

The C1-FFL can be depicted as a network where each link is associated with a signal and each node transforms the input signal(s) into an output signal. Fig. 1a shows the network of C1-FFL. The input signal is $s(t)$ and output signal is $z(t)$. Both $x_*(t)$ and $y_*(t)$ are intermediate signals, and $s_y(t)$ is an external signal.

The C1-FFL in Fig. 1a is an abstraction of the molecular interactions which are depicted in Fig. 1b. In the figure, both S and S_y are inducers. Both X and Y are TFs, which are expressed by their corresponding gene. The inducer S (resp. S_y) turns the inactive form X (Y) into its active form X_* (Y_*). The activation of gene Z requires the binding of both X_* and Y_* to the promoter of Z , i.e. the AND gate in Fig. 1a.

Note that there is a one-to-one correspondence between the chemical species in Fig. 1b with their corresponding time signals in Fig. 1a, e.g. $x_*(t)$ is the concentration of X_* at time t and so on. In this paper, we will assume that the inducer S_y is always present and its concentration is always above the threshold needed to activate Y . Furthermore, we assume the activation of Y by S_y is fast, this allows us to write $y_*(t) = y(t)$ and we will use $y(t)$ for $y_*(t)$ from now on. By using Hill function to model the gene expression, [19] presents

an ODE model for C1-FFL, as follows:

$$\frac{dx_*(t)}{dt} = k_+(M - x_*(t))s(t) - k_-x_*(t) \quad (1a)$$

$$\frac{dy(t)}{dt} = \underbrace{\frac{h_{xy}x_*(t)^{n_{xy}}}{K_{xy}^{n_{xy}} + x_*(t)^{n_{xy}}}}_{H_{xy}(x_*(t))} - d_y y(t) \quad (1b)$$

$$\frac{dz(t)}{dt} = \underbrace{\frac{h_{xz}x_*(t)^{n_{xz}}}{K_{xz}^{n_{xz}} + x_*(t)^{n_{xz}}}}_{H_{xz}(x_*(t))} \times \underbrace{\frac{h_{yz}y(t)^{n_{yz}}}{K_{yz}^{n_{yz}} + y(t)^{n_{yz}}}}_{H_{yz}(y(t))} - d_z z(t) \quad (1c)$$

where k_+ , k_- , d_y and d_z are reaction rate constants; h_{xy} , n_{xy} , K_{xy} , h_{xz} , n_{xz} , K_{xz} , h_{yz} , n_{yz} and K_{yz} are coefficients for Hill functions $H_{xy}(x_*(t))$, $H_{xz}(x_*(t))$ and $H_{yz}(y(t))$. Lastly, $x(t) + x_*(t)$ is the constant M . The multiplication of H_{xz} and H_{yz} on the right-hand side (RHS) of (1c) implements the AND gate in Fig. 1a. With suitably chosen parameter values, the C1-FFL in (1) acts as a persistence detector in the sense that if the input signal $s(t)$ is a persistent (resp. transient), then the output $z(t)$ has a high (low) value.

2.2 Detection theory

Detection theory [16] is a branch of statistical signal processing. Its aim is to use the measured data to decide whether an event of interest has occurred. In the context of this paper, the events are whether the signal is transient or persistent. A detection problem is often formulated as a hypothesis testing problem, where each hypothesis corresponds to a possible event. Let us consider a detection problem with two hypotheses, denoted by \mathcal{H}_0 and \mathcal{H}_1 , which correspond to respectively, the events of transient and persistent signals. Our aim is to decide which hypothesis is more likely to hold. We define the log-likelihood ratio R :

$$R = \log \left(\frac{\text{P}[\text{measured data}|\mathcal{H}_1]}{\text{P}[\text{measured data}|\mathcal{H}_0]} \right) \quad (2)$$

where $\text{P}[\text{measured data}|\mathcal{H}_i]$ is the conditional probability that the measured data is generated according to hypothesis \mathcal{H}_i . Note that we have chosen to use log-likelihood ratio, rather than likelihood ratio, because it will enable us to build a connection with C1-FFL later on. Intuitively, if the log-likelihood ratio R is positive, then the measured data is more likely to have been generated by a persistent signal or hypothesis \mathcal{H}_1 , and vice versa. Therefore, the key idea of detection theory is to use the measured data to compute the log-likelihood ratio and then use it to make a decision.

The likelihood ratio has a close connection to the Neyman-Pearson Lemma in statistics. Let us consider a detection problem where the the hypotheses \mathcal{H}_0 and \mathcal{H}_1 correspond, respectively, to the negative and positive conditions. In this case, the Neyman-Pearson Lemma states that likelihood ratio is the statistical measure that can be used to maximise

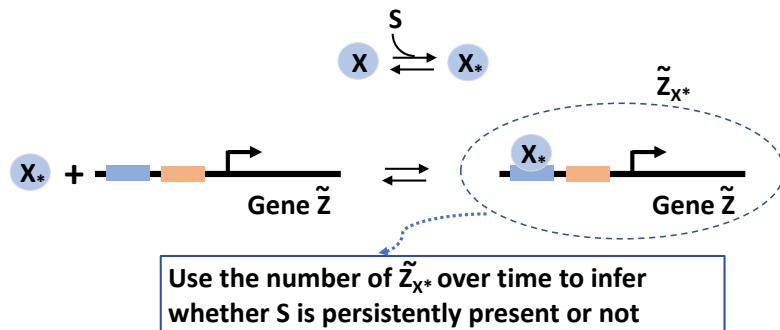


Figure 2: The reaction pathway for the detection problem.

the true positive rate (i.e. the probability of deciding for \mathcal{H}_1 given \mathcal{H}_1 is true) for a given false positive rate (i.e. the probability of deciding for \mathcal{H}_1 given \mathcal{H}_0 is true). We will discuss why likelihood ratio is a relevant measure for some biological detection problems in Sec. 4.3.

3 Statistical detection on a reaction pathway

Our aim is to consider a statistical detection problem to determine whether the input signal is persistent or not. However, in this section, we will consider a more general detection problem because it can readily be solved and we will specialise it to persistence detection in Sec. 4. This section is divided into two parts. We define the detection problem in Sec. 3.1 and present its solution in Sec. 3.2.

Convention: In this paper, we use upper case letters to denote a chemical species, e.g. S, X_* etc. For each chemical species, there are two corresponding continuous-time signals based on its concentration and molecular counts. E.g. for the chemical species X_* , we denote its concentration over time as $x_*(t)$ (note: lower case x) and its molecular counts over time is $X_*(t)$ (note: upper case X).

3.1 Detection problem

In order that we can connect the detection problem to C1-FFL later on, we will define the detection problem using a reaction pathway which is a subset of the C1-FFL species and reactions in Fig. 1b. We have depicted the reaction pathway used in the detection problem in Fig. 2. The reaction pathway consists of five chemical species: S, inactive X and its corresponding active form X_* , as well as inactive \tilde{Z} and the complex \tilde{Z}_{X^*} which is formed by the binding of X_* to \tilde{Z} . These five species take part in the following four

chemical reactions:



where k_+ , k_- , g_+ and g_- are reaction propensity constants. In this paper, we will make the simplifying assumption that the volume scaling needed to convert between propensity and reaction rate constants is 1. This simplification allows us to equate propensity constants with reaction rate constants and there is no loss of generality of the results. With this assumption, note that k_+ and k_- in (3a) and (3b) are equal to those in (1a).

In terms of molecular biology, S is an inducer and X is a TF. In Reaction (3a), the species S activates X to produce X_* . Reaction (3b) is a deactivation reaction. The reactions (3a) and (3b) are depicted in both Figs. 1b and 2.

The species \tilde{Z} is a gene. In fact, \tilde{Z} in Fig. 2 is the same as Z in Fig. 1b. Note that Fig. 1b follows the standard convention in molecular biology where a gene and the protein that it expresses are given the same symbol Z. However, in this paper, we need different symbols for the gene and the protein that the gene expresses so that we can clearly distinguish their corresponding time signals. Therefore, we have chosen to use \tilde{Z} to denote the gene and use Z to denote the protein expressed by \tilde{Z} . In Reaction (3c), an active X_* binds with the promoter of \tilde{Z} to produce the complex \tilde{Z}_{X_*} . Lastly, Reaction (3d) is an unbinding reaction.

Note that we have intentionally chosen the reaction between S and X as an approximate enzymatic reaction rather than a binding reaction so that we can vary the quantity of S independently. This simplifies the detection problem solution and the discussion in this paper.

Let $X(t)$, $X_*(t)$, $\tilde{Z}(t)$ and $\tilde{Z}_{X_*}(t)$ denote, respectively, the *number* of X, X_* , \tilde{Z} and \tilde{Z}_{X_*} molecules at time t . Note the signals $X(t)$, $X_*(t)$, $\tilde{Z}(t)$ and $\tilde{Z}_{X_*}(t)$ are piecewise constant because they are molecular counts. We assume that $X(t) + X_*(t)$ (resp. $\tilde{Z}(t) + \tilde{Z}_{X_*}(t)$) is a constant for all t and we denote this constant by M (N).

We assume that the input signal $s(t)$ is deterministic. We model the reactions (3) using chemical master equation [12], i.e. the reaction system (3) is modelled as a continuous-time Markov chain with state vector $[X(t), X_*(t), \tilde{Z}(t), \tilde{Z}_{X_*}(t)]$.

We have now defined the reaction pathway and its model. We learn from Sec. 2.2 that the definition of a detection problem requires us to specify the measured data and two hypotheses. We will do that next.

The measured datum at time t is $\tilde{Z}_{X_*}(t)$. However, in the formulation of the detection problem, we will assume that at time t , the data available to the detection problem are $\tilde{Z}_{X_*}(\tau)$ for all $\tau \in [0, t]$; in other words, the data are continuous in time and are the history of the counts of \tilde{Z}_{X_*} up to time t inclusively. We will use $\tilde{Z}_{X_*}(t)$ to denote the continuous-time history of $\tilde{Z}_{X_*}(t)$ up to time t inclusively. Note that each history $\tilde{Z}_{X_*}(t)$

is a realisation of a continuous-time Markov chain; this means the same input signal $s(t)$ can result in different $\tilde{Z}_{X_*}(t)$.

The last step in defining the detection problem is to specify the hypotheses \mathcal{H}_i ($i = 0, 1$). Later on, we will identify \mathcal{H}_0 and \mathcal{H}_1 with, respectively, transient and persistent signals. However, at this stage, we want to solve the detection problem in a general way. We assume that the hypothesis \mathcal{H}_0 (resp. \mathcal{H}_1) is that the input signal $s(t)$ is the signal $c_0(t)$ (resp. $c_1(t)$) where $c_0(t)$ and $c_1(t)$ are two different deterministic signals. Intuitively, the aim of the detection problem is to decide which of the two signals $c_0(t)$ and $c_1(t)$ is more likely to have produced the observed history.

We remark that in the definition of the detection problem, the input signal $s(t)$ is not directly observable. Since S reacts with the molecules in the reaction pathway in Fig. 2, the downstream signal $\tilde{Z}_{X_*}(t)$ contains information on $s(t)$. The aim of the detection problem is to infer the information on $s(t)$ from this downstream signal. Given that we model the reaction pathway with chemical master equation, the signal $\tilde{Z}_{X_*}(t)$ is noisy.

3.2 Solution to the detection problem

The aim of the detection problem is to determine which hypothesis \mathcal{H}_i ($i = 0, 1$) is likely to have generated the observed history $\tilde{Z}_{X_*}(t)$. Consider the log-likelihood ratio $L(t)$:

$$L(t) = \log \left(\frac{\text{P}[\tilde{Z}_{X_*}(t)|\mathcal{H}_1]}{\text{P}[\tilde{Z}_{X_*}(t)|\mathcal{H}_0]} \right) \quad (4)$$

where $\text{P}[\tilde{Z}_{X_*}(t)|\mathcal{H}_i]$ is the conditional probability of observing the history $\tilde{Z}_{X_*}(t)$ given hypothesis \mathcal{H}_i .

We show in Appendix A that the time evolution of $L(t)$ is given by the following ODE:

$$\frac{dL(t)}{dt} = \left[\frac{d\tilde{Z}_{X_*}(t)}{dt} \right]_+ \log \left(\frac{J_1(t)}{J_0(t)} \right) - g_+(N - \tilde{Z}_{X_*}(t))(J_1(t) - J_0(t)) \quad (5)$$

$$J_i(t) = \text{E}[X_*(t)|\tilde{Z}_{X_*}(t), \mathcal{H}_i] \quad (6)$$

where $[w]_+ = \max(w, 0)$ is the positive part of w , $\text{E}[\]$ denotes expectation and $\text{E}[X_*(t)|\tilde{Z}_{X_*}(t), \mathcal{H}_i]$ is the conditional expectation of $X_*(t)$ given the history and \mathcal{H}_i . Note that in deriving (5), we assume that $c_i(t)$'s have been properly chosen so that $\log \left(\frac{J_1(t)}{J_0(t)} \right)$ is well defined.

We assume that the two hypotheses are *a priori* equally likely, so $L(0) = 0$. Since $\tilde{Z}_{X_*}(t)$ is a piecewise constant function counting the number of \tilde{Z}_{X_*} molecules, its derivative is a sequence of Dirac deltas at the time instants that \tilde{Z}_{X_*} forms or unbinds. Note that the Dirac deltas corresponding to the formation of \tilde{Z}_{X_*} carries a positive sign and the $[]_+$ operator keeps only these. Fig. 3a shows an example $\tilde{Z}_{X_*}(t)$ and its corresponding $\left[\frac{d\tilde{Z}_{X_*}(t)}{dt} \right]_+$.

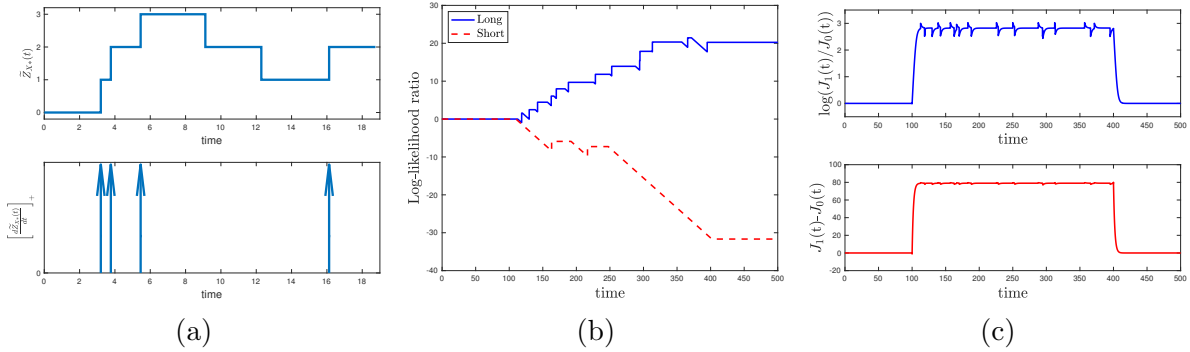


Figure 3: Figures for Sec. 3.2. (a) Illustrating $\tilde{Z}_{X^*}(t)$ and $\left[\frac{d\tilde{Z}_{X^*}(t)}{dt}\right]_+$. (b) The log-likelihood ratio for a long signal (or persistent signal) and a short signal. (c) The top and bottom plots show $\log\left(\frac{J_1(t)}{J_0(t)}\right)$ and $J_1(t) - J_0(t)$ in (5).

We present a numerical example to illustrate the properties of (5) and to explain what information is important for persistence detection.

Numerical example The kinetic parameters for the reaction pathway are: $k_+ = 0.02$, $k_- = 0.5$, $g_+ = 0.002$ and $g_- = 0.002$. The total number of TFs M is 100 and the number of genes N is 1. The reference signal $c_0(t)$ (resp. $c_1(t)$) is a rectangular ON/OFF pulse with an ON duration of 100 (400). The reference signals have an amplitude of 37.5 (resp. 1.31) when it is ON (OFF).

We first use a persistent signal as the input $s(t)$. For simplicity, we choose $s(t)$ to be the same as $c_1(t)$. We use the Stochastic Simulation Algorithm (SSA) [13] to simulate the reaction pathway to obtain a realisation of $\tilde{Z}_{X^*}(t)$. We use optimal Bayesian filtering to obtain $E[X_*(t)|\tilde{Z}_{X^*}(t), \mathcal{H}_i]$ for both $i = 0, 1$. We then numerically integrate (5) to obtain the log-likelihood ratio $L(t)$, which is plotted as the solid blue line in Fig. 3b. We see that the log-likelihood ratio is zero for $t \leq 100$, ramps up in the time interval $[100, 400]$ and plateaus after $t \geq 400$. The log-likelihood ratio reaches a positive value at the end, which means correct detection because it says the input $s(t)$ is more likely to be similar to the reference signal $c_1(t)$.

Next, we use a transient signal as $s(t)$ and we choose $s(t)$ to be $c_0(t)$. We perform the same steps as before, namely SSA simulation, optimal Bayesian filtering and numerical integration to obtain the log-likelihood ratio for this transient input. The resulting $L(t)$ is plotted as red dashed lines in Fig. 3b. This $L(t)$ becomes negative which again means correct detection.

Fig. 3c shows the weighting factors $\log\left(\frac{J_1(t)}{J_0(t)}\right)$ and $J_1(t) - J_0(t)$ in (5) for the case when the input $s(t)$ is $c_1(t)$. (The curves are similar when $s(t)$ is $c_0(t)$.) It shows that these two weighting factors are mostly positive in the time interval $[100, 400]$ but are zero outside. This means the contribution to the log-likelihood ratio comes from the signal within $[100, 400]$. This can also be seen from Fig. 3b where the log-likelihood ratio does not change outside of $[100, 400]$ but increases (resp. decreases) for persistent (transient)

signal within [100,400]. This makes intuitive sense because the persistent input is different from the transient input within this time interval, so the signal in this time interval is useful for discriminating persistent signals from transient ones. We remark that the deterministic C1-FFL model in [1] also has a zero initial time response.

If a persistent signal can give a large positive log-likelihood ratio, then the probability of correctly detecting the persistent signal is higher. For this example, the positive contribution to log-likelihood ratio comes from the first term on the RHS of (5) because the weighting factors are non-negative, see Fig. 3c. In fact, each time when a X_* binds to a \tilde{Z} in the time interval [100,400], it creates a positive jump in the magnitude of the log-likelihood ratio, which can be seen in Fig. 3b. This means that a persistent signal becomes easier to detect if X_* binds to \tilde{Z} many times when the signal is ON. This can be achieved if the ON duration of the persistent signal has a longer time-scale compared to those of the binding and unbinding reactions of \tilde{Z}_{X_*} (i.e. reactions (3c) and (3d)) so that these reactions occur many times when the input is ON.

4 Compute log-likelihood ratio approximately

Our ultimate goal is to show that the computation of the log-likelihood ratio $L(t)$ in (5) can be carried out by a C1-FFL in (1), i.e. there exists a set of parameters for the C1-FFL such that $z(t)$ in (1) is approximately equal to $L(t)$ in (5). It is not obvious from the expression of (5) that this can be done. The aim of this section is to derive an ODE, which will be referred to as the **intermediate approximation**, such that the output of this ODE is approximately equal to $L(t)$ when the input is persistent. We will then use this intermediate approximation in Sec. 5 to relate to C1-FFL.

4.1 Assumptions

The detection problem and its solution in Sec. 3 are general in the sense that they apply to any reaction pathways of the form (3), reference signals $c_i(t)$ and input signal $s(t)$. In order to connect the detection problem to the C1-FFL model in (1), we will need to make specific assumptions to derive the intermediate approximation. We will specify these assumptions in this subsection.

We make the following two assumptions on the reaction pathway (3):

- The time-scale of the inducer-TF reactions (3a) and (3b) is faster than that of the TF-gene promoter reactions (3c) and (3d).
- The number of TF molecules M is much higher than the number of genes N .

We believe these are realistic assumptions. First, according to [1, Table 2.1], for *E. coli*, the time-scale for equilibrium binding of small molecules to protein is of the order of 1 ms and the time-scale for TF binding to gene promoter is of the order of 1s. Second, the copy number of most genes is either 1 or 2.

In order to use mathematical methods to derive the intermediate approximation, we assume that the input signal $s(t)$ is a rectangular pulse with the following temporal profile:

$$s(t) = \begin{cases} a & \text{for } 0 \leq t < d \\ a_0 & \text{otherwise} \end{cases} \quad (7)$$

where d is the pulse duration, and a is the pulse amplitude when it is ON and a_0 is the basal concentration of the inducer with $a > a_0 > 0$. In order to show that the intermediate approximation is general, we will show that it holds for a range of a and d values. We say that an input signal $s(t)$ is persistent if its amplitude a is sufficiently high and its duration d is sufficiently long; otherwise, the signal is transient.

For analytical tractability, we choose $c_0(t)$ and $c_1(t)$ to be rectangular pulses. We assume that when the reference signal is ON, its concentration level is a_1 ; and when it is OFF, its concentration level is at the basal level a_0 with $a_1 > a_0$. The temporal profile of $c_i(t)$ (where $i = 0, 1$) is:

$$c_i(t) = \begin{cases} a_1 & \text{for } 0 \leq t < d_i \\ a_0 & \text{otherwise} \end{cases} \quad (8)$$

where d_i is the duration of the pulse $c_i(t)$. In particular, we assume that the duration of $c_1(t)$ is longer than $c_0(t)$, i.e. $d_1 > d_0$. We can therefore identify $c_0(t)$ and $c_1(t)$ as the reference signals for, respectively, the transient and persistent signals.

For the derivation of the intermediate approximation, we need two technical conditions. First, the amplitude a_1 has to be sufficiently large so that $\frac{Mk_+a_1}{Mk_+a_1+k_-}$ is large compared to the number of genes N . This is so that we can approximate $J_0(t)$ and $J_1(t)$ in (5) by simpler expressions. Second, we assume that if a persistent input is applied to the reaction pathway (3), the pathway is at steady state by d_0 . This requirement can be met if the duration d_0 is long enough. It may be instructive to recall from the discussion in the numerical example in Sec. 3.2 that there is a time interval which is informative for persistence detection. For the assumptions in this section, the informative time interval can be shown to be $[d_0, \min(d, d_1)]$. Ultimately, this assumption, together with others, allow us to use the steady state statistics in the time interval $[d_0, \min(d, d_1)]$ to “replace” $\left[\frac{d\tilde{Z}_{X^*}(t)}{dt}\right]_+$ and $g_+(N - \tilde{Z}_{X^*}(t))$ in (5) by, respectively, $g_- \tilde{Z}_{X^*}(t)$ and $g_- \frac{\tilde{Z}_{X^*}(t)}{X^*(t)}$. Note that we have on purpose put double quotes around the word replace to alert the reader to the fact that the replacement expressions are only heuristically, not mathematically, equivalent.

4.2 Intermediate approximation

An ideal persistence detector has the properties that a transient input will result in a zero output and a persistent input will result in a positive output [1]. The C1-FFL, when acting as a persistence detector, can be considered to be an approximation of this ideal behaviour [1]. However, it is not possible to map the log-likelihood ratio detector in (5) to C1-FFL because the log-likelihood ratio becomes negative for transient signals but the concentration

in C1-FFL can only be non-negative. A purpose of the intermediate approximation is to compute only the positive part of the log-likelihood ratio, which happens when the input is persistent. Another purpose of the intermediate approximation is to replace the complex computation in (5), e.g. derivative and optimal Bayesian filtering, by simpler computation that can be implemented by chemical reactions. The intermediate approximation has two key properties. First, if the input is transient, then the output of the intermediate approximation is zero. Second, if the input is persistent, then the output of the intermediate approximation is approximately equal to the log-likelihood ratio given by (5).

The derivation of the intermediate approximation is given in Appendix B, making use of the assumptions stated in Sec. 4.1. The derivation shows that the time evolution of the intermediate approximation $\hat{L}(t)$ is given by the following ODE:

$$\frac{d\hat{L}(t)}{dt} = \tilde{Z}_{X_*}(t) g_- \pi(t) [\phi(X_*(t))]_+ \quad (9)$$

$$\text{where } \phi(X_*(t)) = \log\left(\frac{X_1}{X_0}\right) - \frac{X_1 - X_0}{X_*(t)}, \quad (10)$$

$$X_i = \frac{Mk_+a_i}{k_+a_i + k_-} \text{ for } i = 0, 1 \quad (11)$$

$$\pi(t) = \begin{cases} 1 & \text{for } d_0 \leq t < d_1 \\ 0 & \text{otherwise} \end{cases} \quad (12)$$

$$\hat{L}(0) = 0 \quad (13)$$

Furthermore, it can be shown that time evolution of $E[\hat{L}(t)]$ obeys the following ODE:

$$\frac{dE[\hat{L}(t)]}{dt} = E[\tilde{Z}_{X_*}(t)] g_- \pi(t) [\phi(E[X_*(t)])]_+ \quad (14)$$

The behaviour of the intermediate approximation $\hat{L}(t)$ depends on the amplitude a and duration d of the input signal $s(t)$. Three important properties for $\hat{L}(t)$ are:

1. If $d < d_0$, then for all t , we have $\hat{L}(t)$ and $E[\hat{L}(t)]$ are zero or small. This is due to $\pi(t)$, which is zero outside of $[d_0, d_1)$, and the fact that $X_*(t)$ is likely to be small for $t \geq d_0$.
2. If the amplitude a is lower than a threshold, then for all t , we have $\hat{L}(t)$ is zero or small and $E[\hat{L}(t)]$ is zero. We will explain this for $E[\hat{L}(t)]$. Since $E[X_*(t)]$ is an increasing function of a , this means a small a will give a small $E[X_*(t)]$. If $E[X_*(t)]$ is less than $\frac{X_1 - X_0}{\log\left(\frac{X_1}{X_0}\right)}$ for all t , then $[\phi(E[X_*(t)])]_+$ on the RHS of (14) is zero and this implies $E[\hat{L}(t)]$ is zero for all t . The explanation for $\hat{L}(t)$ is similar.
3. If d is longer than d_0 and a is sufficiently large, then for $0 \leq t < \min\{d, d_1\}$ we have $\hat{L}(t) \approx L(t)$ where $L(t)$ is given in (5).

The first two properties are concerned with transient signals, which are those input signals whose duration is no longer than d_0 or whose amplitude a is small. The intermediate approximation says that transient signals give a small $\hat{L}(t)$. On the other hand, persistence signals have a duration longer than d_0 and have a sufficiently large amplitude a . For persistent signals, the intermediate approximation $\hat{L}(t)$ is approximately equal to the log-likelihood ratio $L(t)$ in the time interval $0 \leq t < \min\{d, d_1\}$. From now on, we will choose d_1 to be ∞ so that $\hat{L}(t) \approx L(t)$ holds for $0 \leq t < d$, i.e. when the persistent signal is ON. Note that an infinite d_1 means $\pi(t)$ in (9) becomes a step function which changes from 0 to 1 at time d_0 .

4.2.1 Numerical examples and the advantages of using $\hat{L}(t)$

The numerical examples in this section use the following kinetic parameters for the reaction pathway: $k_+ = 0.02$, $k_- = 0.5$, $g_+ = 0.002$ and $g_- = 0.05$. These parameters have been chosen such that the time-scale of the inducer-TF reactions are faster than those of the TF-gene promoter. The number of genes N is 1. The parameters for the reference signals are: $d_0 = 100$, $d_1 = \infty$, $a_0 = 1.3158$ and $a_1 = 131.57$. All the above parameters are fixed. The parameters that we will vary are M , a and d .

For the first numerical experiment, we use $M = 600$ for the reaction pathway, and $a = 37.5$ (which gives a 0.6 probability that the \tilde{Z} is bound) and $d = 800$ for the input signal. We use SSA simulation to generate 100 realisations of $X_*(t)$ and $\tilde{Z}_{X_*}(t)$, and use them to compute the true log-likelihood ratio $L(t)$ (which requires only $\tilde{Z}_{X_*}(t)$) and the intermediate approximation $\hat{L}(t)$ (which requires both $X_*(t)$ and $\tilde{Z}_{X_*}(t)$). We then compute over these 100 realisations: the mean of $L(t)$, the mean of $\hat{L}(t)$, and the root-mean-square (RMS) error of $L(t) - \hat{L}(t)$. The results are plotted in Fig. 4a. It shows that the mean of $L(t)$ is close to that of $\hat{L}(t)$ in the time interval $[0, 800]$, which is the duration of the input signal. At time $t = 800$, we have mean of $L(t) = 45.7$, mean of $\hat{L}(t) = 49.2$ and RMS error is 12.2. The large RMS error between $L(t)$ and $\hat{L}(t)$ is because $L(t)$ is a much noisier than $\hat{L}(t)$. Figs. 4b and 4c show the mean and standard deviation of, respectively, $L(t)$ and $\hat{L}(t)$. We can summarise our observations so far as: $\hat{L}(t)$ is a slightly biased estimate of $L(t)$ but at the same time having a much smaller variance.

Next, we use the same parameters as before except $a = 16.67$ which gives a 0.4 probability that the \tilde{Z} is bound. We again use 100 SSA simulations to obtain the mean of $L(t)$, the mean of $\hat{L}(t)$, and the RMS error of $L(t) - \hat{L}(t)$. Fig. 4d shows the mean of $\hat{L}(t)$ again approximates that of the mean of $L(t)$. At $t = 800$, we have mean of $L(t) = 24.9$ and mean of $\hat{L}(t) = 26.6$, which means the bias is small. The RMS error in Fig. 4d is large because $L(t)$ is very noisy; this is understandable because a smaller a makes the input signal harder to detect. The vertical bars in Fig. 4d shows the standard deviation of $\hat{L}(t)$. An important point to note is that the standard deviation of $\hat{L}(t)$ is small.

Based on the above numerical results, we want to argue that there is an advantage in using $\hat{L}(t)$, instead of $L(t)$, for detection. The key advantage of using $\hat{L}(t)$ is that it has a far lower variance. If we think about our detection problem setup, we start with a deterministic input $s(t)$ and generate many realisations of $X_*(t)$ and $\tilde{Z}_{X_*}(t)$, and then use

them to compute the likelihood ratio or the intermediate approximation. Ultimately, our setup is deterministic because for each deterministic input $s(t)$, we want to say whether $s(t)$ is persistent or not. This means for each $s(t)$, we should expect only one answer. However, for our setup, because of the infinite number of realisations of $X_*(t)$ and $\tilde{Z}_{X_*}(t)$, each $s(t)$ gives an infinite number of answers. We can therefore view the lower variance of $\hat{L}(t)$ as a way of getting almost one answer from $s(t)$. Since $s(t)$ is deterministic, the variance in $L(t)$ and $\hat{L}(t)$ is caused by the intrinsic noise in $X_*(t)$ and $\tilde{Z}_{X_*}(t)$. Therefore, another advantage of using $\hat{L}(t)$ is that it is less affected by intrinsic noise. Having discussed the advantages of using $\hat{L}(t)$, we should point out that the biasedness of $\hat{L}(t)$ may result in more false positives or false negatives compared to $L(t)$. However, this may be a worthwhile price to pay because $\hat{L}(t)$ is less affected by intrinsic noise.

The above numerical results show that $\hat{L}(t)$ has a lower variance compared to $L(t)$. This can be explained intuitively. The computation of $L(t)$ makes use of $\tilde{Z}_{X_*}(t)$ alone while that of $\hat{L}(t)$ uses both $X_*(t)$ and $\tilde{Z}_{X_*}(t)$. The use of an additional upstream signal, i.e. $X_*(t)$, is an advantage according to the information processing inequality from information theory [10].

Next we study how the parameters M and d impact on the bias and variance of $\hat{L}(t)$. We know from the derivation of the intermediate approximation in Appendix B that $\hat{L}(t)$ better approximates $L(t)$ when M increases; we will verify that. In the first set of numerical experiments, we use $a = 37.5$, $d = 800$ and choose M from $\{100, 200, \dots, 600\}$. For each M , we obtain 100 realisations of the reaction pathway signals and use them to compute $L(t)$ and $\hat{L}(t)$. We define relative bias of $\hat{L}(t)$ at time t as $\frac{|E[\hat{L}(t)] - L(t)|}{E[L(t)]}$. The upper plot of Fig. 4e graphs the relative bias of $\hat{L}(t)$ and coefficient of variation (CV) of $\hat{L}(t)$ at $t = d$ for different M 's. It shows that both relative bias and CV decreases with increasing M . In the next set of numerical experiments, we use $a = 37.5$, $M = 300$ and d from $\{200, 300, 400, \dots, 1200\}$. The lower plot of Fig. 4e shows the relative bias and CV of $\hat{L}(t)$ at $t = d$. We see that relative bias and CV becomes smaller with increasing d .

Finally, we check the accuracy of using (14) to compute $E[\hat{L}(t)]$. Fig. 4f plots the mean of $\hat{L}(t)$ obtained from two methods: (i) The average of $\hat{L}(t)$ computed from 100 SSA simulations; (ii) $E[\hat{L}(t)]$ computed from (14). The two curves in Fig. 4f overlap with each other; this shows that (14) is an accurate method to compute $E[\hat{L}(t)]$.

Remark: The reader may wonder why we do not define the hypotheses of the detection problem as: \mathcal{H}_0 (resp. \mathcal{H}_1) means the duration of the input signal is shorter (longer) than a given threshold. The reason is that these are composite hypotheses and the solution to the resulting detection problem is much harder, see [7, Remark 5.1] for a more in-depth discussion. We also want to point that, even with our simpler formulation, the resulting detector gives a small output for any signal whose duration is shorter than d_0 .

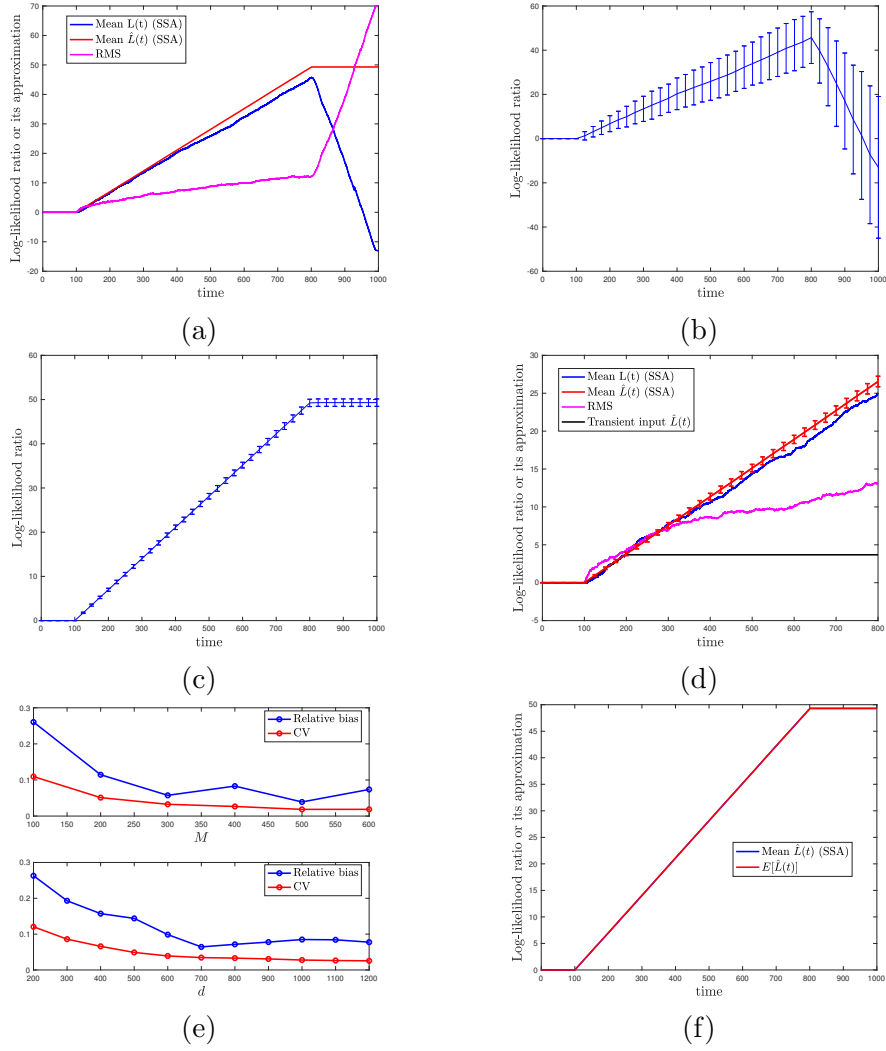


Figure 4: Numerical results for Sec. 4.2. (a) Comparing the mean of $L(t)$ and mean of $\hat{L}(t)$; and RMS error between $L(t)$ and $\hat{L}(t)$. (b) Mean and standard deviation of $L(t)$. (c) Mean and standard deviation of $\hat{L}(t)$. (d) Similar to subfigure (a) but for a smaller value of a . (e) Impact of M and d on relative bias and CV of $\hat{L}(t)$. (f) Comparing the mean of $\hat{L}(t)$ obtained from SSA against $E[\hat{L}(t)]$ computed by (14). Note that the two lines overlap.

4.3 Relevance to biological detection problems

In this section, we will discuss why the likelihood ratio is a relevant criterion for some biological detection problems. For this exposition, we will assume that the purpose of the detection is to determine if a certain food is persistently present and if yes, then the organism wants to produce the enzyme to consume the food. Our discussion is based on Bayesian decision theory which considers both utility and cost of actions, e.g. the successful detection and consumption of a food gives a positive utility to the organism at the cost of producing the enzyme.

We will use the hypotheses \mathcal{H}_0 and \mathcal{H}_1 to refer to the conditions that the food is respectively, absent and present, in the environment. We will also use negative and positive, respectively, to refer to the two hypotheses \mathcal{H}_0 and \mathcal{H}_1 . Given these two hypotheses, the detection problem may decide for either \mathcal{H}_0 (negative) or \mathcal{H}_1 (positive). Table 1 summarises the four possible combinations from the two environmental conditions and the two detection outcomes. These four combinations are labelled as True Negative (TN), False Negative (FN), False Positive (FP) and True Positive (TP) using the terminologies commonly used in statistics. For the time being, we assume that the utility can only take two values: U_1 and U_0 where $U_1 > U_0 = 0$. The living organism can only get the positive utility U_1 for TP as this is the only situation which the food is present and detected. Similarly, for the cost, we assume $C_1 > C_0 = 0$. The living organism incurs a cost when FP or TP occurs as enzymes are made in these cases.

Let P_0 and P_1 denote the true probabilities that the food is, respectively, absent and present. Let also P_{TP} denote the probability of TP etc. The mean utility is $P_{TP}P_1U_1$ and the mean cost is $P_{FP}P_0C_1 + P_{TP}P_1C_1$. Let C_{\max} be the maximum cost that the living organism can afford. From a Bayesian decision point of view, the goal is to maximise the mean utility subject to a constraint on the mean cost, i.e.

$$\begin{aligned} \max P_{TP}P_1U_1 \\ \text{subject to } P_{FP}P_0C_1 + P_{TP}P_1C_1 \leq C_{\max} \end{aligned} \tag{15}$$

We show in Appendix D that the solution of this utility maximisation problem is to choose a suitable positive threshold ρ such that the organism should decide for \mathcal{H}_1 if the likelihood ratio $\frac{P[\text{data}|\mathcal{H}_1]}{P[\text{data}|\mathcal{H}_0]} \geq \rho$. In fact, the derivation shows that, if $U_1 > \lambda C_1$ where λ is the Lagrangian multiplier of the above optimisation problem, then the above utility maximisation problem is equivalent to maximising P_{TP} subject to an upper bound on P_{FP} , which is in fact the scenario covered by the Neyman-Pearson lemma. This shows that the likelihood ratio is a suitable statistic to be used. Note that we have assumed for simplicity that $U_0 = 0$ and $C_0 = 0$ earlier, however it can be shown that, under some conditions, the result still holds for non-zero U_0 and C_0 .

We use a numerical example to illustrate the impact of the positive decision threshold ρ on the TP and FP rates. For the TP rate, we assume the input is a long pulse of duration $d = 800$ and generate 100 realisations of $X_*(t)$ and $\tilde{Z}_{X_*}(t)$. We use the data to compute 100 values of $L(d)$ and $\hat{L}(d)$ where $L(d)$ and $\hat{L}(d)$ are, respectively, the log-likelihood ratio (5) and approximate log-likelihood ratio (9) at time $t = d$. We then compare these values

		Environmental conditions	
		Negative	Positive
Detection outcomes	Negative	True Negative (TN) Utility = U_0 Cost = C_0	False Negative (FN) Utility = U_0 Cost = C_0
	Positive	False Positive (FP) Utility = U_0 Cost = C_1	True Positive (TP) Utility = U_1 Cost = C_1

Table 1: The utilities and costs of the four combinations of environmental conditions and detection outcomes.

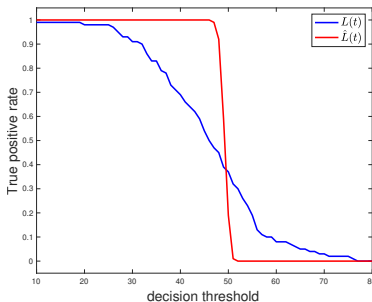


Figure 5: The impact of the decision threshold on the TP rates.

against the threshold to obtain the TP rates. We vary the threshold between 10 and 80. Fig. 5 shows that there is a wide range of thresholds that can be used to obtain a high TP rate for $\hat{L}(t)$ but not for $L(t)$. This is because $\hat{L}(t)$ has a lower variance in comparison.

For the FP rate, we generate 100 realisations using a short pulse of duration $d = 100 (= d_0)$ and use the data to compute $L(d)$ and $\hat{L}(d)$. For all the 100 realisations, the $L(d)$'s are negative and $\hat{L}(t) \approx 0$. Therefore for all the thresholds in 10 – 80, the FP rates are zero for both $\hat{L}(t)$ and $L(t)$. This shows that we are able to find thresholds that give a large TF while keeping FP low.

The above numerical experiment on computing the FP rate also shows that it is not a problem to “round” the negative log-likelihood ratio in $L(d)$ to a near zero approximation $\hat{L}(d)$. This is because, if the test is to check whether the log-likelihood ratio is above a sufficiently positive threshold, then a negative $L(d)$ or an almost zero $\hat{L}(d)$ will lead to the same decision.

5 Using C1-FFL to approximately compute log-likelihood ratio

We have shown in the previous section that the mean of the intermediate approximation $E[\hat{L}(t)]$ is an accurate approximation of the mean log-likelihood ratio $E[L(t)]$ when the

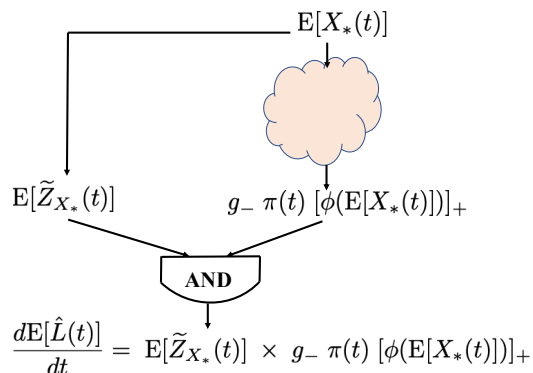


Figure 6: Relating the computation of the mean approximate log-likelihood ratio $E[\hat{L}(t)]$ in (14) to C1-FFL.

input is persistent. The aim of this section is to show that we can use the C1-FFL in (1) to approximately compute $E[\hat{L}(t)]$ in (14).

5.1 Relating $E[\hat{L}(t)]$ to C1-FFL

For the time being, we will assume d_z in (1c) is zero and show that $z(t)$ in (1) can be made approximately equal to $E[\hat{L}(t)]$ in (14). We will explain in Remark 1 how a non-zero d_z can be handled.

We depict the calculations of (14) in Fig. 6. We split the computation on the RHS of (14) as the product of $E[\tilde{Z}_{X_*}(t)]$ and $g_- \pi(t) [\phi(E[X_*(t)])]_+$ where the multiplication operation is depicted as an AND gate in the figure. Note that the two-branch structure of the computation in Fig. 6 has a direct resemblance with that of the C1-FFL in Fig. 1. We first consider the computation of the two branches separately.

We first consider the computation of $E[\tilde{Z}_{X_*}(t)]$ from $E[X_*(t)]$, which is the branch on the left in Fig. 6. By using the volume scaling assumption (Sec. 3), we equate molecular count $\tilde{Z}_{X_*}(t)$ with concentration $\tilde{z}_{X_*}(t)$, and similarly, $X_*(t)$ with $x_*(t)$. We propose to compute $\tilde{z}_{X_*}(t)$ from $x_*(t)$ by using:

$$\tilde{z}_{X_*}(t) \stackrel{\text{computed by}}{=} \frac{Ng_+x_*(t)}{g_+x_*(t) + g_-} \quad (16)$$

By using the reaction rate constants of the reaction pathway (3) in the numerical example in Section 4.2.1, we have plotted the two sides of (16) in Fig. 7a when the input is persistent with a duration d of 200. Note that there are two transients of $\tilde{z}_{X_*}(t)$ in the figure, one after time 0 when the input turns ON and the other at time d when the input turns OFF. We can see that, other than these two transients, the two sides of (16) are almost equal. We will show later on these two transients have little effect on the accuracy of the overall

computation. Note that the RHS of (16) has the form of a Hill function and we can identify it with $H_{xz}(x_*(t))$ in (1c).

We next consider the computation of $g_- \pi(t) [\phi(E[X_*(t)])]_+$ from $E[X_*(t)]$, which is depicted by a cloud in Fig. 6. We first argue that, for most of the admissible choices of d_0 , there must be a time delay element in the cloud. This implies that there must be some chemical reactions in the cloud in order to create this time delay. To understand which d_0 is admissible, we recall that we assume in Section 4.1 that the pathway (3) is at steady state by the time d_0 . As an illustration of this assumption, consider Fig. 7a which shows the time profile of $\tilde{z}_{X_*}(t)$, the vertical dashed line shows the time (which we will denote as t_{ss}) by which $\tilde{z}_{X_*}(t)$ is sufficiently close to steady state, the assumption means an admissible d_0 must be greater than or equal to t_{ss} .

In Appendix E, we show that there must be a delay in the cloud if d_0 is strictly greater than t_{ss} . Intuitively, a delay is needed because $\pi(t)$ is zero in $[0, d_0)$ but X_* reaches steady state before d_0 . Given that there must be a delay element in the cloud in Fig. 6, we can achieve that by inserting a transcription node (e.g. Node Y in Fig. 1) in the cloud. With this insertion, we can identify the branch on the right in Fig. 6 with the indirect branch in C1-FFL in Fig. 1.

The next step is to show that we can find Hill functions $H_{xy}()$ and $H_{yz}()$ in (1) which will enable us to compute $g_- \pi(t) [\phi(x_*(t))]_+$. The argument is focused on the duration $t < d$. Since the inducer-TF pathway is fast, therefore, we can assume that for $t < d$, we can equate $x_*(t)$ to its steady state value x_* . We can use (1b) to show that

$$y(t) = \frac{H_{xy}(x_*)}{d_y} (1 - \exp(-d_y t)) \quad (17)$$

Our aim is to achieve the approximation:

$$H_{yz}(y(t)) \approx g_- \pi(t) [\phi(x_*)]_+ \quad (18)$$

We first note that in the above approximation, $y(t)$ is an increasing function of t and $\pi(t)$ is a step. If $H_{yz}()$ is a Hill function of the form in (1c), we now argue that we can find h_{yz} , n_{yz} and K_{yz} such that:

$$\frac{y(t)^{n_{yz}}}{K_{yz}^{n_{yz}} + y(t)^{n_{yz}}} \approx \pi(t) \quad (19)$$

$$h_{yz} \approx g_- [\phi(x_*)]_+ \quad (20)$$

We first consider (19) where we aim to approximate the step function $\pi(t)$ which changes from 0 to 1 at d_0 . Since $y(t)$ is an increasing function, if we choose K_{yz} to be $y(d_0)$, then we have $y(t) < K_{yz}$ for $t < d_0$ and $y(t) > K_{yz}$ for $t > d_0$. Next, if n_{yz} is sufficiently large, then the LHS (19) will rise from 0 to (nearly) 1 over time around d_0 . In order that slight change in K_{yz} will not destroy this approximation, it would be helpful to choose reaction rate constant d_y in (17) so that $y(t)$ is not close to steady state at d_0 . This shows we can find K_{yz} and n_{yz} so (19) holds. For a given value of x_* , (20) shows how h_{yz} can be chosen.

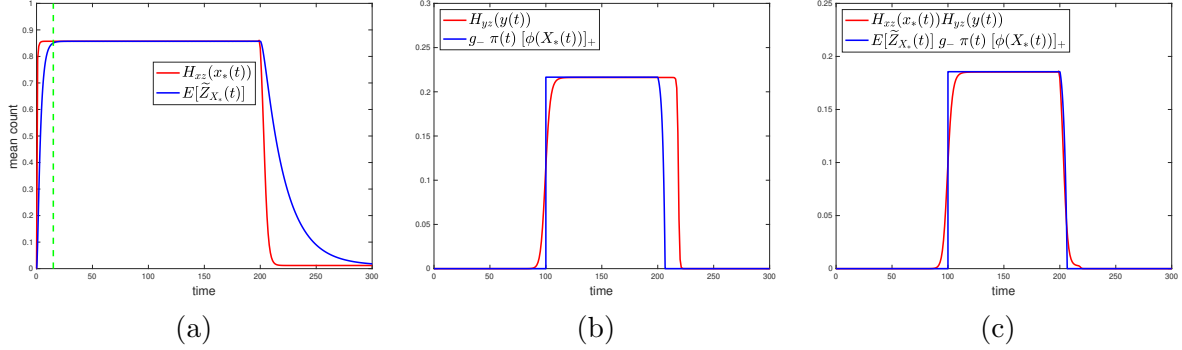


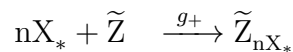
Figure 7: (a) Comparing $\tilde{z}_{X_*}(t)$ and $\frac{Ng_{+}x_*(t)}{g_{+}x_*(t)+g_{-}}$. (b) Comparing $g_{-} \pi(t) [\phi(x_*)]_{+}$ and $H_{yz}(y(t))$. (c) Comparing $\tilde{z}_{X_*}(t)g_{-} \pi(t) [\phi(x_*)]_{+}$ and $H_{xz}(x_*(t))H_{yz}(y(t))$.

The above argument works for a particular value of x_* which also corresponds to a particular value of input signal amplitude. We now argue that we can choose the Hill function parameters such that the approximations (19) and (20) hold for a range of input amplitudes which is equivalent to a range of x_* . First, if $H_{xy}(x_*)$ is a Hill function, then for sufficiently large x_* , the value of $H_{xy}(x_*)$ does not change much because $H_{xy}(x_*)$ saturates. As a result, there is a range of x_* such that $y(t)$ does not change a lot. This means if we choose K_{yz} to be the $y(d_0)$ corresponding to a particular x_* which saturates $H_{xy}(x_*)$, we can continue to obtain an approximation of the step function $\pi(t)$ for a range of x_* . Second, note that the function $[\phi(x_*)]_{+}$ flattens out if x_* is sufficiently large, therefore h_{yz} can be chosen so that (20) holds for a range of x_* . Overall, this means we can choose the parameters of the Hill functions H_{xy} and H_{yz} so that (18) holds for a range of input amplitudes. Fig. 7b plots the two sides of (18) for a particular input amplitude. We see that we can use H_{yz} to approximate $g_{-} \pi(t) [\phi(x_*)]_{+}$ well except near the rising and falling edges of $g_{-} \pi(t) [\phi(x_*)]_{+}$. Note that this example is for a particular value of x_* , we will present an example that works for a range of x_* in Sec. 5.2.

After considering the two branches in Fig. 6 separately. We now compare the whole RHS of (14), which is $E[\tilde{Z}_{X_*}(t)]$ times $g_{-} \pi(t) [\phi(E[X_*(t)])]_{+}$, and the RHS of (1c), which is $H_{xy}(x_*(t))$ times $H_{yz}(y(t))$. Fig. 7c compares these two expressions. An interesting observation is that the mismatch in some time intervals in Fig. 7a and 7b are cancelled out when the multiplication is made.

Remark 1 We have shown that if d_z in (1c) is zero, then $z(t)$ in (1) can be made approximately equal to $E[\hat{L}(t)]$ in (14). If d_z in (1c) is non-zero, then we will need to add the term $-d_z E[\hat{L}(t)]$ to the RHS of (14) so that $z(t)$ is approximately equal to $E[\hat{L}(t)]$.

Remark 2 The above argument can be straightforwardly be generalised to the case if the reaction (3c) is changed to the cooperative reaction:



where n molecules of X_* is bind to the gene \tilde{Z} .

5.2 Numerical example

This numerical example uses the same fixed parameter values as in Sec. 4.2.1. Our aim is to show that we can choose a set of C1-FFL parameters so that $z(t) \approx \hat{L}(t)$ for a range of input amplitude a . We do this by fixing $H_{xz}()$ as $\frac{Ng+x_*(t)}{g+x_*(t)+g_-}$, and by fitting the C1-FFL parameters in $H_{xy}()$ and $H_{yz}()$ in (1) by nonlinear optimisation. The data for fitting is obtained from varying a from 3.125 to 62.5 while fixing $M = 300$ and $d = 800$. For each a , we compute $E[\hat{L}(t)]$ using (14) and use them to fit the parameters of the C1-FFL. The fitted values of the C1-FFL parameters are: $k_{xy} = 4.5$, $n_{xy} = 1.01$, $K_{xy} = 2.25$, $d_y = 0.0177$, $h_{yz} = 0.216$, $n_{yz} = 128.3$ and $K_{yz} = 206.8$.

Fig. 8a compares $E[L(t)]$ and C1-FFL output for three different values of a : 5.0, 12.5 and 20.0. It can be seen that they match very well. Next, we compare the value of $z(t)$ and $\hat{L}(t)$ at time $t = 800$ for $a \in [12.5, 100]$. Fig. 8b shows that the match is good for $a \leq 50$ but gets poorer for $a > 50$.

Although we use optimisation to obtain the parameters of the Hill functions $H_{xy}()$ and $H_{yz}()$. We find that their values are compatible to our intuitive argument in Sec. 5.1. First, we say that K_{yz} should be chosen close to the value of $y(d_0)$ for a range of input amplitudes. For input amplitudes of 2.8, 25 and 225 (which correspond to a mean probability of 0.1, 0.5 and 0.9 that the promoter \tilde{Z}_{X^*} is bound), the values of $y(d_0)$ are respectively, 194.7, 206.1 and 207.4. These values are pretty close to $K_{yz} = 206.8$ from using optimization. Second, according to (20), h_{yz} should be chosen as $g_- [\phi(x_*)]_+$. For large x_* , the value of $[\phi(x_*)]_+$ is $\log\left(\frac{X_1}{X_0}\right)$ by (10). The limiting value of $g_- [\phi(x_*)]_+$ is calculated to be 0.226 which is closed to $h_{yz} = 0.216$ from optimization. Third, the steady state value of $y(t)$ is around 250 for a range of input amplitudes and $y(d_0)$ has not yet reached the steady state.

5.3 Discussion

1. In [7], we consider an inducer-TF reaction pathway and study how we can use the counts of active TFs to infer whether the inducer signal is persistent or not. We show that the persistence detector is a C1-FFL but this C1-FFL has the same form as (1) except that the Hill function $H_{xz}(x_*(t))$ in (1c) is replaced by $x_*(t)$. However, this paper shows that persistence detection over an inducer-TF-gene promotor pathway will give rise to the C1-FFL with the structure given in (1). This shows that there is a dependence on the structure of biochemical circuit on the associated signal processing problem.
2. Our interpretation of C1-FFL as a statistical persistence detector shows an interesting signal processing architecture involving parallel processing. The C1-FFL has two arms. The short arm produces the signals $X_*(t)$ and $\tilde{Z}_{X^*}(t)$ which contain information on whether the inducer signal is persistent or not. The longer arm then makes use of the signals $X_*(t)$ and $\tilde{Z}_{X^*}(t)$ to approximately compute, in a parallel manner, the positive part of the log-likelihood ratio. It is also interesting to see that the gene \tilde{Z} ,

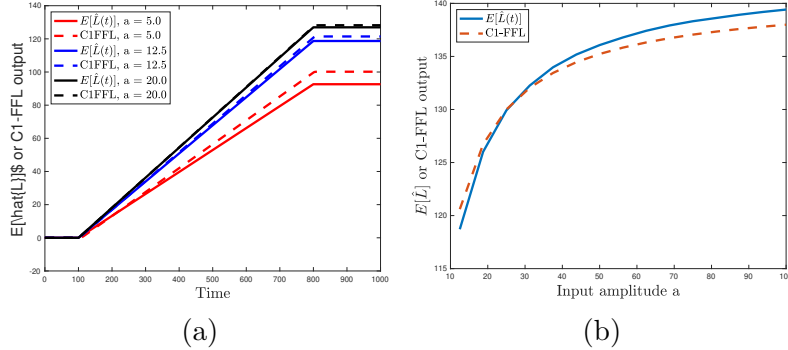


Figure 8: Numerical results for Sec. 5. (a) Comparing the C1-FFL output against $E[\hat{L}(t)]$ for three different values of a . (b) Compare $z(t)$ (C1-FFL) and $\hat{L}(t)$ at time $t = 800$ for $a \in [12.5, 100]$.

with its two promoter sites, has the dual roles of generating the signal to be processed as well as processing the signal.

- There are two interesting open problems that we would like to point out. First, the separation of the $X_*(t)$ and $\tilde{Z}_{X_*}(t)$ factors on the RHS of (14) has allowed us to match (14) to the AND gate in C1-FFL. We learn from the derivation of the intermediate approximation in Appendix B that this separation comes from a result which says that the probability distributions of the counts of $X_*(t)$ and $\tilde{Z}_{X_*}(t)$ are approximately independent. Instead of this approximation on independence, an interesting alternative is to attempt to derive an intermediate approximation which takes the dependence between the counts $X_*(t)$ and $\tilde{Z}_{X_*}(t)$ into consideration. After that, one may try to fit it to an alternative form C1-FFL where the RHS of (1c) is replaced by a factor of, say, the form $\frac{x_*(t)^{n_{xz}} y(t)^{n_{yz}}}{K_0 + K_{xz} x_*(t)^{n_{xz}} + K_{yz} y(t)^{n_{yz}} + K_{xyz} x_*(t)^{n_{xz}} y(t)^{n_{yz}}}$ which is not separable in $x_*(t)$ and $y(t)$; see [4] for how non-independent binding of TFs to multiple promoter sites can be modelled. This may be able to reduce the bias in $E[\hat{L}(t)]$. Second, we have managed to fit $E[\hat{L}(t)]$ to a deterministic model of C1-FFL. An open problem is to fit to a stochastic model of C1-FFL.
- In this paper, we have shown that we can use the C1-FFL to approximately compute the positive part of log-likelihood ratio. An alternative is to find a molecular circuit that can approximately compute the decision metric of likelihood ratio. An interesting open question is understand the properties of these two decision metrics in a cellular environment.

6 Conclusions and discussion

In this paper, we show that the biochemical circuit C1-FFL can be used as a statistical detector of persistent signals. Our method consists of two steps. In the first step, we

formulate a statistical detection problem over an inducer-TF-gene pathway and derive its solution in terms of computing the log-likelihood ratio. After that, in the second step, we derive a method to approximately compute the log-likelihood ratio and show that it can be implemented by a C1-FFL. The method for the first step is based on Markovian theory and is fairly standard. The bulk of the work for this paper lies in the second step where we derive a method to approximately compute the log-likelihood ratio. Comparing with our previous work [7] where we consider the persistence detection over an inducer-TF pathway, the derivation of the approximate log-likelihood ratio computation in this paper is a lot more involved. In [7], we only have to consider one random variable which is the number of active TFs. However, in this paper, we need to consider the joint probability distribution of the number of active TFs and the number of complexes formed by the binding of the active TF to the gene promoter.

This paper considers the problem of detecting persistent signals, which can be considered to be a particular case of temporal signal processing in living cells, see [25] for a review. Another example of temporal signal processing in cells is the decoding of concentration modulated signals. We show in [8] that we can also use a method similar to this paper to derive a molecular circuit which can decode concentration modulated signals. We consider a TF-gene reaction pathway where the TF signal is modelled by an ON-OFF pulse with an unknown ON amplitude a . For the detection problem, the observations are the counts of bound gene promoters over time and the hypothesis is that the input has a reference amplitude a_* . The decoding can be realised by a molecular circuit which approximately computes the log-likelihood of seeing the observations given the hypothesis. This circuit has the property that if the input amplitude a is the same as a_* , then the circuit expresses a higher amount of protein compared to other circuits that have a reference amplitude different from a_* . We show in [8] that the molecular circuit derived by our method is consistent with the *S. cerevisiae* DCS2 promoter data in [15], which were obtained from exciting the promoter by using various transcription factor dynamics, e.g. concentration modulation, duration modulation and others.

The concept of likelihood ratio (or a similar quantity) has been used to understand how cells make decision in [17, 27] and how they may estimate concentration of one or more ligands in [11, 23]. We can view the methodology of this paper, together with [11, 17, 27, 23, 7, 8], in a unified manner. Their methodology is to define an information processing problem, solve it and then consider its implementation as a molecular circuit. Interestingly, this methodology has a direct parallel with Marr’s tri-level analysis [21]. Although Marr’s analysis was originally proposed to understand cognitive systems, it has recently been used to understand non-neuron based biological information processing in developmental biology [20]. Marr’s proposal is to understand a computation system at three levels: computational (What is the goal of the computation?), algorithmic (How does it solve the problem?) and implementation (What is the substrate? What are the mechanisms?) For this paper, the computation has the goal to detect persistent signals, the algorithm is to compute the positive part of the log-likelihood ratio and the implementation at the molecular circuit level is C1-FFL. (Lower levels of implementation, e.g. at the molecular and chemical reaction level, are certainly of interest but is not covered by the

methodology in this paper.) We envisage that we can use Marr’s analysis to understand information processing in natural biochemical circuits as well as to design novel information processing circuits. We do that by varying the choices that we make at each of three Marr’s levels. For computational, we can vary the information processing problems, e.g. persistence detection, decoding concentration modulated signal etc. For algorithmic, we can choose to compute log-likelihood ratio, likelihood ratio, posteriori probability etc. For implementation, we can consider gene circuits, protein circuits, neural circuits etc. This paper can be viewed as a particular instantiation of using Marr’s analysis to understand information processing in a natural biochemical circuit.

References

- [1] U. Alon. *An Introduction to Systems Biology: Design Principles of Biological Circuits*. Chapman & Hall, 2006.
- [2] Ehab M Ammar, Xiaoyi Wang, and Christopher V Rao. Regulation of metabolism in *Escherichia coli* during growth on mixtures of the non-glucose sugars: arabinose, lactose, and xylose. *Scientific Reports*, pages 1–11, January 2018.
- [3] Hamdan Awan and Chun Tung Chou. Generalized Solution for the Demodulation of Reaction Shift Keying Signals in Molecular Communication Networks. *IEEE Transactions on Communications*, 65(2):715–727, February 2017.
- [4] Lacramioara Bintu, Nicolas E Buchler, Hernan G Garcia, Ulrich Gerland, Terence Hwa, Jané Kondev, and Rob Phillips. Transcriptional regulation by the numbers: models. *Current opinion in genetics & development*, 15(2):116–124, April 2005.
- [5] Yang Cao, Daniel T Gillespie, and Linda R Petzold. The slow-scale stochastic simulation algorithm. *The Journal of Chemical Physics*, 122(1):014116–19, January 2005.
- [6] Chun Tung Chou. Maximum a-posteriori decoding for diffusion-based molecular communication using analog filters. *IEEE Transactions on Nanotechnology*, 14(6):1054–1067, 2015.
- [7] Chun Tung Chou. Detection of persistent signals and its relation to coherent feed-forward loops. *Royal Society Open Science*, 5(11), November 2018.
- [8] Chun Tung Chou. Designing Molecular Circuits for Approximate Maximum a Posteriori Demodulation of Concentration Modulated Signals. *IEEE Transactions on Communications*, 67(8):5458–5473, July 2019.
- [9] Chun Tung Chou. Using detection theory and molecular computation to understand signal processing in living cells. *2018 52nd Asilomar Conference on Signals, Systems, and Computers*, pages 1822–1826, February 2019.

- [10] T. Cover and J. Thomas. *Elements of Information Theory*. Wiley, 1991.
- [11] Robert G Endres and Ned S Wingreen. Maximum likelihood and the single receptor. *Physical review letters*, 103, 2009.
- [12] C. Gardiner. *Stochastic methods*. Springer, Berlin, Germany, 2010.
- [13] D Gillespie. Exact stochastic simulation of coupled chemical reactions. *The journal of physical chemistry*, 1977.
- [14] Carlos A Gómez-Uribe, George C Verghese, and Abraham R Tzafiriri. Enhanced identification and exploitation of time scales for model reduction in stochastic chemical kinetics. *The Journal of Chemical Physics*, 129(24):244112–17, December 2008.
- [15] Anders S Hansen and Erin K O’Shea. Promoter decoding of transcription factor dynamics involves a trade-off between noise and control of gene expression. *Molecular systems biology*, 9:1–14, November 2013.
- [16] Steve M. Kay. *Fundamentals of Statistical Signal Processing, Volume II: Detection Theory*. Prentice Hall, 1998.
- [17] Tetsuya J Kobayashi and Atsushi Kamimura. Dynamics of intracellular information decoding. *Physical Biology*, 8(5):055007, August 2011.
- [18] S Mangan and U Alon. Structure and function of the feed-forward loop network motif. *Proceedings of the National Academy of Sciences of the United States of America*, 100(21):11980–11985, October 2003.
- [19] S Mangan, A Zaslaver, and U Alon. The Coherent Feedforward Loop Serves as a Sign-sensitive Delay Element in Transcription Networks. *Journal of molecular biology*, 334(2):197–204, November 2003.
- [20] Santosh Manicka and Michael Levin. The Cognitive Lens: a primer on conceptual tools for analysing information processing in developmental and regenerative morphogenesis. *Phil. Trans. R. Soc. B*, 374(1774):20180369–18, June 2019.
- [21] David Marr. *Vision: a computational investigation into the human representation and processing of visual information*. MIT Press, Cambridge, MA, 1982.
- [22] R Milo, S Shen-Orr, S Itzkovitz, N Kashtan, D Chklovskii, and U Alon. Network motifs: simple building blocks of complex networks. *Science*, 298(5594):824–827, October 2002.
- [23] Thierry Mora. Physical Limit to Concentration Sensing Amid Spurious Ligands. *Physical review letters*, 115(3):038102–5, July 2015.
- [24] K Oishi and E Klavins. Biomolecular implementation of linear I/O systems. *Systems Biology, IET*, 5(4):252–260, July 2011.

- [25] Jeremy E Purvis and Galit Lahav. Encoding and Decoding Cellular Information through Signaling Dynamics. *Cell*, 152(5):945–956, February 2013.
- [26] Shai S Shen-Orr, Ron Milo, Shmoolik Mangan, and Uri Alon. Network motifs in the transcriptional regulation network of *Escherichia coli*. *Nature genetics*, 31(1):64–68, April 2002.
- [27] Eric D Siggia and Massimo Vergassola. Decisions on the fly in cellular sensory systems. *Proceedings of the National Academy of Sciences*, 110(39):E3704–12, September 2013.
- [28] D Soloveichik, G Seelig, and E Winfree. DNA as a universal substrate for chemical kinetics. *Proceedings of the National Academy of Sciences of the United States of America*, 107(12):5393–5398, March 2010.
- [29] Niranjana Srinivas, James Parkin, Georg Seelig, Erik Winfree, and David Soloveichik. Enzyme-free nucleic acid dynamical systems. *Science*, 358(6369):2052–2011, December 2017.

A Proof of (5)

Recalling that $\tilde{\mathcal{Z}}_{X^*}(t)$ is the history of $\tilde{Z}_{X^*}(t)$ in the time interval $[0, t]$. In order to derive (5), we consider the history $\tilde{\mathcal{Z}}_{X^*}(t + \Delta t)$ as a concatenation of $\tilde{\mathcal{Z}}_{X^*}(t)$ and $\tilde{Z}_{X^*}(t)$ in the time interval $(t, t + \Delta t]$. We assume that Δt is chosen small enough so that no more than one reaction can take place in $(t, t + \Delta t]$. Given this assumption and right continuity of continuous-time Markov Chains, we can use $\tilde{Z}_{X^*}(t + \Delta t)$ to denote the history of $\tilde{Z}_{X^*}(t)$ in $(t, t + \Delta t]$.

Consider the likelihood of observing the history $\tilde{\mathcal{Z}}_{X^*}(t + \Delta t)$ given hypothesis \mathcal{H}_i :

$$\text{P}[\tilde{\mathcal{Z}}_{X^*}(t + \Delta t)|\mathcal{H}_i] \quad (21)$$

$$= \text{P}[\tilde{\mathcal{Z}}_{X^*}(t) \text{ AND } \tilde{Z}_{X^*}(t + \Delta t)|\mathcal{H}_i] \quad (22)$$

$$= \text{P}[\tilde{\mathcal{Z}}_{X^*}(t)|\mathcal{H}_i] \text{P}[\tilde{Z}_{X^*}(t + \Delta t)|\mathcal{H}_i, \tilde{\mathcal{Z}}_{X^*}(t)] \quad (23)$$

where we have expanded $\tilde{\mathcal{Z}}_{X^*}(t + \Delta t)$ in (21) using concatenation.

By using (23) in the definition of log-likelihood ratio, we can show that:

$$L(t + \Delta t) = L(t) + \log \left(\frac{\text{P}[\tilde{Z}_{X^*}(t + \Delta t)|\mathcal{H}_1, \tilde{\mathcal{Z}}_{X^*}(t)]}{\text{P}[\tilde{Z}_{X^*}(t + \Delta t)|\mathcal{H}_0, \tilde{\mathcal{Z}}_{X^*}(t)]} \right) \quad (24)$$

The expression $\text{P}[\tilde{Z}_{X^*}(t + \Delta t)|\mathcal{H}_i, \tilde{\mathcal{Z}}_{X^*}(t)]$ is the prediction of the number of \tilde{Z}_{X^*} molecules at time $t + \Delta t$ based on its history up till time t . We can obtain $\text{P}[\tilde{Z}_{X^*}(t + \Delta t)|\mathcal{H}_i, \tilde{\mathcal{Z}}_{X^*}(t)]$ by solving an optimal Bayesian filtering problem on the continuous-time Markov chain that models the dynamics of the reactions (3a)–(3d). By using the method of [3], we have

$$\begin{aligned} & \text{P}[\tilde{Z}_{X^*}(t + \Delta t)|\mathcal{H}_i, \tilde{\mathcal{Z}}_{X^*}(t)] = \\ & \delta_{\tilde{Z}_{X^*}(t+\Delta t), \tilde{Z}_{X^*}(t)+1} g_+(N - \tilde{Z}_{X^*}(t)) J_i(t) \Delta t + \\ & \delta_{\tilde{Z}_{X^*}(t+\Delta t), \tilde{Z}_{X^*}(t)-1} g_- \tilde{Z}_{X^*}(t) \Delta t + \\ & \delta_{\tilde{Z}_{X^*}(t+\Delta t), \tilde{Z}_{X^*}(t)} \times \\ & (1 - g_+(N - \tilde{Z}_{X^*}(t))J_i(t) \Delta t - g_- \tilde{Z}_{X^*}(t) \Delta t) \end{aligned} \quad (25)$$

where $\delta_{a,b}$ is the Kronecker delta which is 1 when a equals to b and zero otherwise, and $J_i(t) = \mathbf{E}[X_*(t)|\mathcal{H}_i, \tilde{\mathcal{Z}}_{X^*}(t)]$ is the expected number of X_* molecules at time t given Hypothesis i and the history $\tilde{\mathcal{Z}}_{X^*}(t)$.

Note that $\text{P}[\tilde{Z}_{X^*}(t + \Delta t)|\mathcal{H}_i, \tilde{\mathcal{Z}}_{X^*}(t)]$ in (25) is a sum of three terms with multipliers $\delta_{\tilde{Z}_{X^*}(t+\Delta t), \tilde{Z}_{X^*}(t)+1}$, $\delta_{\tilde{Z}_{X^*}(t+\Delta t), \tilde{Z}_{X^*}(t)-1}$ and $\delta_{\tilde{Z}_{X^*}(t+\Delta t), \tilde{Z}_{X^*}(t)}$. Since these multipliers are

mutually exclusive, we have:

$$\begin{aligned}
& \log \left(\frac{\mathbb{P}[\tilde{Z}_{X_*}(t + \Delta t) | \mathcal{H}_1, \tilde{Z}_{X_*}(t)]}{\mathbb{P}[\tilde{Z}_{X_*}(t + \Delta t) | \mathcal{H}_0, \tilde{Z}_{X_*}(t)]} \right) \\
&= \delta_{\tilde{Z}_{X_*}(t+\Delta t), \tilde{Z}_{X_*}(t)+1} \log \left(\frac{g_+(N - \tilde{Z}_{X_*}(t)) J_1(t) \Delta t}{g_+(N - \tilde{Z}_{X_*}(t)) J_0(t) \Delta t} \right) + \\
& \quad \delta_{\tilde{Z}_{X_*}(t+\Delta t), \tilde{Z}_{X_*}(t)-1} \log \left(\frac{g_- \tilde{Z}_{X_*}(t) \Delta t}{g_- \tilde{Z}_{X_*}(t) \Delta t} \right) + \\
& \quad \delta_{\tilde{Z}_{X_*}(t+\Delta t), \tilde{Z}_{X_*}(t)} \times \\
& \quad \log \left(\frac{1 - g_+(N - \tilde{Z}_{X_*}(t)) J_1(t) \Delta t - g_- \tilde{Z}_{X_*}(t) \Delta t}{1 - g_+(N - \tilde{Z}_{X_*}(t)) J_0(t) \Delta t - g_- \tilde{Z}_{X_*}(t) \Delta t} \right) \\
& \approx \delta_{\tilde{Z}_{X_*}(t+\Delta t), \tilde{Z}_{X_*}(t)+1} \log \left(\frac{J_1(t)}{J_0(t)} \right) - \\
& \quad \delta_{\tilde{Z}_{X_*}(t+\Delta t), \tilde{Z}_{X_*}(t)} g_+(N - \tilde{Z}_{X_*}(t)) (J_1(t) - J_0(t)) \Delta t \tag{26}
\end{aligned}$$

where we have used the approximation $\log(1 + f \Delta t) \approx f \Delta t$ and have ignored terms of order $(\Delta t)^2$ or higher to obtain (26). Note also that the above derivation assumes that $\frac{J_1(t)}{J_0(t)}$ is strictly positive so its logarithm is well defined; this can be achieved by properly choosing $c_i(t)$'s.

By substituting (26) into (24), we have after some manipulations and after taking the limit $\Delta t \rightarrow 0$:

$$\begin{aligned}
\frac{dL(t)}{dt} &= \lim_{\Delta t \rightarrow 0} \frac{\delta_{\tilde{Z}_{X_*}(t+\Delta t), \tilde{Z}_{X_*}(t)+1}}{\Delta t} \log \left(\frac{J_1(t)}{J_0(t)} \right) - \\
& \quad \delta_{\tilde{Z}_{X_*}(t+\Delta t), \tilde{Z}_{X_*}(t)} g_+(N - \tilde{Z}_{X_*}(t)) (J_1(t) - J_0(t)) \tag{27}
\end{aligned}$$

In order to obtain (5), we use the following reasonings. First, the term $\lim_{\Delta t \rightarrow 0} \frac{\delta_{\tilde{Z}_{X_*}(t+\Delta t), \tilde{Z}_{X_*}(t)+1}}{\Delta t}$ is a Dirac delta at the time instant that an X_* molecule is bind with \tilde{Z} . Second, the term $\delta_{\tilde{Z}_{X_*}(t+\Delta t), \tilde{Z}_{X_*}(t)}$ is only zero when the number of \tilde{Z}_{X_*} molecule changes but the number of such changes is countable. In other words, $\delta_{\tilde{Z}_{X_*}(t+\Delta t), \tilde{Z}_{X_*}(t)} = 1$ with probability one. This allows us to drop $\delta_{\tilde{Z}_{X_*}(t+\Delta t), \tilde{Z}_{X_*}(t)}$. Hence (5). We remark that a more general framework of deriving log-likelihood ratio in the reaction-diffusion master equation framework can be found in [6].

B Proof of (9)

The aim of this section is to show that the log-likelihood ratio computation in (5) can be approximated by the intermediate approximation in (9) for persistent signals in the time

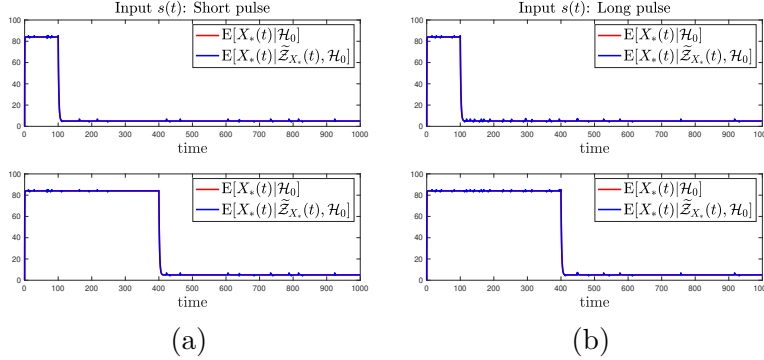


Figure 9: Comparing $E[X_*(t)|\tilde{\mathcal{Z}}_{X_*}(t), \mathcal{H}_i]$ and $E[X_*(t)|\mathcal{H}_i]$. Top plot: $i = 0$; Bottom plot: $i = 1$. (a) Input $s(t)$ is short. (b) Input $s(t)$ is long.

interval $[0, \min(d, d_1)]$. The derivation is based on the assumptions stated in Sec. 4.1. We have divided the derivation into four steps. We will provide a numerical example at the end of this section to demonstrate the properties of these approximation steps.

(Step 1) The aim of this step is to approximate $E[X_*(t)|\tilde{\mathcal{Z}}_{X_*}(t), \mathcal{H}_i]$ in (5). The computation of this expectation requires the solution of a Bayesian optimal filtering problem which is computationally intensive. In this step, we use the approximation:

$$E[X_*(t)|\tilde{\mathcal{Z}}_{X_*}(t), \mathcal{H}_i] \approx E[X_*(t)|\mathcal{H}_i]. \quad (28)$$

From probability theory, we know that for three random variables A , B and C , we have $E_C[E[A|B, C]] = E[A|B]$. This means that the RHS of (28) is the mean of the LHS side over all possible histories of $\tilde{\mathcal{Z}}_{X_*}(t)$. Alternatively, we can view this approximation as replacing the filtering problem by using prior knowledge of the hypotheses.

We use a numerical example to demonstrate the accuracy of this approximation. We use the same parameter values in the example in Sec. 3.2. Fig. 9 plots $E[X_*(t)|\tilde{\mathcal{Z}}_{X_*}(t), \mathcal{H}_i]$ and $E[X_*(t)|\mathcal{H}_i]$ for $i = 0, 1$ and for a short input (Fig. 9a) and for a long input (Fig. 9b). Note that the curve for $E[X_*(t)|\tilde{\mathcal{Z}}_{X_*}(t), \mathcal{H}_i]$ is almost on top of $E[X_*(t)|\mathcal{H}_i]$.

(Step 2) In this step, we use the signal waveform of the reference signals $c_i(t)$ to obtain the following approximation:

$$E[X_*(t)|\mathcal{H}_0] \approx \begin{cases} X_1 & \text{for } 0 \leq t < d_0 \\ X_0 & \text{otherwise} \end{cases} \quad (29)$$

$$E[X_*(t)|\mathcal{H}_1] \approx \begin{cases} X_1 & \text{for } 0 \leq t < d_1 \\ X_0 & \text{otherwise} \end{cases} \quad (30)$$

where

$$X_i = \frac{Mk_+a_i}{k_+a_i + k_-} \text{ for } i = 0, 1. \quad (31)$$

Let us first recall that a_1 (resp. a_0) is the amplitude of the reference signal when it is ON (OFF). The quantity X_i in (31) is the steady state mean number of X_* molecules when the reference signal is a_i assuming that none of the X_* has bound to the gene \tilde{Z} . We will now argue why we can neglect the number of X_* molecules that have bound to \tilde{Z} . First, let us consider the case when the reference signal amplitude is a_1 . If a_1 has been chosen to be sufficiently large and if $M \gg N$ (i.e. the number of TF X molecules ($= M$) is much greater than the number of genes \tilde{Z} ($= N$)), then the number of X_* will be far bigger than the number of genes. This allows us to neglect the X_* that are bound to \tilde{Z} . Next, let us consider the case when the reference signal amplitude is a_0 , which is a basal quantity. For a small a_0 , the number of X_* is small. Furthermore, with a small number of genes and a small propensity rate g_+ , the chance of X_* binding to the gene is negligible. This justifies (31).

By invoking the assumption that the reactions (3a) and (3b) are fast, we have (29) and (30).

After using the approximations in Steps 1 and 2, (5) becomes:

$$\frac{dL(t)}{dt} \approx \left[\frac{d\tilde{Z}_{X_*}(t)}{dt} \right]_+ \log \left(\frac{X_1}{X_0} \right) \pi(t) - g_+(N - \tilde{Z}_{X_*}(t))(X_1 - X_0) \pi(t) \quad (32)$$

where $\pi(t)$ is defined in (12).

(Step 3) Note that the RHS of (32) is the sum of two terms that do not depend on $L(t)$. We can therefore consider the contribution of each term to $L(t)$ separately.

First, we consider the contribution of the first term on the RHS of (32) to $L(t)$, which we will call $L_1(t)$:

$$\frac{dL_1(t)}{dt} = \left[\frac{d\tilde{Z}_{X_*}(t)}{dt} \right]_+ \log \left(\frac{X_1}{X_0} \right) \pi(t) \quad (33)$$

By integrating the above equation and by using (29) and (30), we have for $t \in [0, d_0)$, $L_1(t) = 0$ and for $t \in [d_0, \min(d, d_1)]$:

$$L_1(t) = \log \left(\frac{X_1}{X_0} \right) \int_{d_0}^t \left[\frac{d\tilde{Z}_{X_*}(\tau)}{d\tau} \right]_+ d\tau \quad (34)$$

If d_0 is long enough so that the reaction pathway (3) reaches steady state by d_0 , then the above equation can be written as:

$$L_1(t) \approx \log \left(\frac{X_1}{X_0} \right) R_{\tilde{Z}_{X_*}} (t - d_0) \quad (35)$$

where $R_{\tilde{Z}_{X_*}}$ is the mean rate at which the binding of X_* to \tilde{Z} (i.e. reaction (3c)) occurs. It can be shown that, at steady state, the mean binding rate $R_{\tilde{Z}_{X_*}}$ is equal to the mean unbinding rate of \tilde{Z}_{X_*} , which is g_- times the mean number of \tilde{Z}_{X_*} . By using ergodicity, we have for $t \in [d_0, \min(d, d_1)]$:

$$L_1(t) \approx \log\left(\frac{X_1}{X_0}\right) \int_{d_0}^t g_- \tilde{Z}_{X_*}(\tau) d\tau \quad (36)$$

Therefore, in differential form, we have

$$\frac{dL_1(t)}{dt} \approx g_- \tilde{Z}_{X_*}(t) \log\left(\frac{X_1}{X_0}\right) \pi(t) \quad (37)$$

Next, we consider the contribution of the second term on the RHS of (32) to $L(t)$, which we will call $L_2(t)$:

$$\frac{dL_2(t)}{dt} = g_+(N - \tilde{Z}_{X_*}(t))(X_1 - X_0) \pi(t) \quad (38)$$

By integrating the above equation, we have $L_2(t) = 0$ for $t \in [0, d_0]$; for $t \in [d_0, \min(d, d_1)]$, we have:

$$L_2(t) = (X_1 - X_0) g_+ \int_{d_0}^t (N - \tilde{Z}_{X_*}(\tau)) d\tau \quad (39)$$

Since the reaction pathway is in steady state in the time interval $[d_0, \min(d, d_1)]$, we can replace the time average in (39) by its ensemble average. In this part, we will overload the symbol \tilde{Z}_{X_*} to use it to refer to the random variable of the number of \tilde{Z}_{X_*} molecules at steady state. This should not cause any confusion because the meaning should be clear from the context. In addition, we will overload the symbol X_* in the same way. With this overloading, the mean number of X_* and \tilde{Z}_{X_*} molecules at steady state are denoted by $E[X_*]$ and $E[\tilde{Z}_{X_*}]$ respectively. We can now rewrite (39) as:

$$L_2(t) \approx (X_1 - X_0) g_+(N - E[\tilde{Z}_{X_*}]) (t - d_0) \quad (40)$$

In order to be able to connect to C1-FFL, we will need to replace the expression $(N - E[\tilde{Z}_{X_*}])$ by a different expression. The derivation of this replacement expression requires a few auxiliary results.

(Auxiliary Result 1) By considering the global balance of the steady state of the reaction pathway (3), we have:

$$g_+ E[(N - \tilde{Z}_{X_*}) X_*] = g_- E[\tilde{Z}_{X_*}] \quad (41)$$

(Auxiliary Result 2) Since the inducer-TF reactions are faster than the TF-gene reactions and $M \gg N$, we can show that the joint probability distribution of X_* and \tilde{Z}_{X_*} , which is denoted by $p(X_*, \tilde{Z}_{X_*})$, can be approximated by:

$$p(X_*, \tilde{Z}_{X_*}) \approx B(X_*; M, k_+ a) B(\tilde{Z}_{X_*}; N, g_+ X_a) \quad (42)$$

where $X_a = \frac{Mk_+a}{k_+a+k_-}$, and $B(Q; m, f)$ denotes that the random variable Q has a binomial distribution with parameters m (number of trials) and f (success probability). We prove this approximation in Appendix C by using the method in [14] to write down two master equations for the fast and slow variables. Here we provide an intuitive argument based on [5]. First, the fast-scale dynamics is almost independent of the slow dynamics because it is at the beginning of the pathway and $M \gg N$, so the distribution of X_* is approximately binomial distributed. Second, consider a duration over which the number of unbound gene promoter \tilde{Z} is a constant. In this duration, the number of X_* fluctuates but the effective reaction rate at which gene promoters are bound is equal to the number of unbound promoter times $g_+ E[X_*]$. Therefore, at steady state, the random variable \tilde{Z}_{X_*} also has a binomial distribution.

(Auxiliary Result 3) Consider binomial distribution $B(Q; m, f)$, then for sufficiently large m and f , we have

$$\frac{1}{E[Q]} \approx E\left[I\left(\frac{1}{Q}\right)\right] \quad (43)$$

where

$$I\left(\frac{1}{q}\right) = \begin{cases} 0 & \text{for } q = 0 \\ \frac{1}{q} & \text{for } q \geq 1 \end{cases} \quad (44)$$

This result essentially says that the mean of the reciprocal of a binomial random variable (with $\frac{1}{0}$ excluded) is approximately equal to the reciprocal of the mean of the binomial random variable. If $f = 1$ and $m \geq 1$, the binomial distribution has a single outcome with a non-zero probability so (43) is exact. Intuitively, if a probability has a single modal distribution with a narrow spread, then (43) holds approximately. For $f = 0.1$, the relative error of using (43) is 3.21% for $m = 300$ and drops to 1.87% for $m = 500$. Similarly, for $f = 0.3$, the relative error is 0.79% for $m = 300$ and drops to 0.47% for $m = 500$. In general, the approximation is better for large m and f .

We will now use the above auxiliary results and (40) to derive the replacement expression. By applying Auxiliary Result 2, which says that the probability distribution of X_* and \tilde{Z}_{X_*} are almost independent to the RHS of (41), we have:

$$g_+ E[(N - \tilde{Z}_{X_*})] \approx g_- E[\tilde{Z}_{X_*}] \frac{1}{E[X_*]} \quad (45)$$

We then apply Auxiliary Result 3 to the RHS of (45) to obtain:

$$g_+ \mathbb{E}[(N - \tilde{Z}_{X_*})] \approx g_- \mathbb{E}[\tilde{Z}_{X_*}] \mathbb{E}[I(\frac{1}{X_*})] \quad (46)$$

By applying Auxiliary Result 2 to the RHS of (46), we have:

$$g_+ \mathbb{E}[(N - \tilde{Z}_{X_*})] \approx g_- \mathbb{E}[\tilde{Z}_{X_*} I(\frac{1}{X_*})] \quad (47)$$

By substituting (47) into (40), we have:

$$L_2(t) \approx (X_1 - X_0) g_- \mathbb{E}[\tilde{Z}_{X_*} I(\frac{1}{X_*})](t - d_0) \quad (48)$$

By turning the above equation into the differential form, we have:

$$\frac{dL_2(t)}{dt} \approx (X_1 - X_0) g_- \tilde{Z}_{X_*}(t) I(\frac{1}{X_*(t)}) \pi(t) \quad (49)$$

Next, by combining (37) and (49), we have:

$$\frac{dL(t)}{dt} \approx g_- \tilde{Z}_{X_*}(t) \pi(t) \left\{ \log \left(\frac{X_1}{X_0} \right) - (X_1 - X_0) I(\frac{1}{X_*(t)}) \right\} \quad (50)$$

(Step 4) Since a set of chemical reactions can be modelled by a set of ODEs, we want to turn the ODE in (50) into a form that can be implemented by a set of chemical reactions. However, (50) cannot be directly implemented by chemical reactions because log-likelihood ratio can take both positive and negative values but chemical concentration is always non-negative. Although [24] has derived a chemical computation system that can have both positive and negative numbers but it requires double the number of species and reactions. As in our previous work [8], we choose to compute only positive part of the log-likelihood ratio. We do that by applying $[\]_+$ to the RHS of (50); we have:

$$\begin{aligned} \frac{dL(t)}{dt} \approx g_- \tilde{Z}_{X_*}(t) \pi(t) \times \\ \left[\log \left(\frac{X_1}{X_0} \right) - (X_1 - X_0) I(\frac{1}{X_*(t)}) \right]_+ \end{aligned} \quad (51)$$

We now replace $I(\frac{1}{X_*(t)})$ in (51) by $\frac{1}{X_*(t)}$ to obtain:

$$\begin{aligned} \frac{dL(t)}{dt} \approx g_- \tilde{Z}_{X_*}(t) \pi(t) \times \\ \left[\log \left(\frac{X_1}{X_0} \right) - (X_1 - X_0) \frac{1}{X_*(t)} \right]_+ \end{aligned} \quad (52)$$

	Step 1	Step 2	Step 3	Step 4
RMS error	1.5	1.9	12.4	12.4
Relative bias (%)	3.1	3.8	7.4	7.4
CV	0.256	0.256	0.017	0.017

Table 2: This table compares the RMS error, relative bias and CV for the four steps of approximation.

The removal of $I(\cdot)$ will not make much difference because the probability of having $X_*(t)$ equals to 0 is small when the input signal is persistent. Note that (52) is the same as (9). This completes the derivation for (9).

In order to derive (14), we start from (52) and take expectation on both sides. If the amplitude a is sufficiently high, then there is a high probability that $X_*(t)$ is large. This means we can take the expectation operator to the inside of the $[\cdot]_+$ operator. After that we apply Auxiliary Results 2 and 3 to obtain (14).

(Numerical example) The aim of this numerical example is to illustrate the properties of the four approximation steps. We use the same fixed parameters as in Sec. 4.2.1. The other parameters are $M = 600$, $a = 37.5$ and $d = 800$. Let $\hat{L}_i(t)$ (for $i = 1, \dots, 4$) be the approximation obtained after Step i ; note that $\hat{L}_4(t)$ is the same as $\hat{L}(t)$. We use 100 realisations from SSA simulations to compute $L(t)$ and $\hat{L}_i(t)$. We compute the RMS error of $\hat{L}_i(t) - L(t)$, relative bias $\frac{|\mathbb{E}[\hat{L}_i(t) - L(t)]|}{\mathbb{E}[L(t)]}$ and CV of $\hat{L}_i(t)$ at $t = d$. The results are shown in Table 2.

The results show that $\hat{L}_1(t)$ and $\hat{L}_2(t)$ are very similar to $L(t)$ because of their small RMS error, while $\hat{L}_3(t)$ and $\hat{L}_4(t)$ have similar properties. Since $\hat{L}_4(t)$ is the same as $\hat{L}(t)$, we can conclude that the approximations in Step 3 cause an increase in relative bias and a decrease in CV. Note that $\hat{L}_2(t)$ is computed using $\tilde{Z}_{X_*}(t)$ only, but $\hat{L}_3(t)$ is computed using computed using $X_*(t)$ and $\tilde{Z}_{X_*}(t)$. Intuitively, the use of $X_*(t)$ may help reduce to reduce the CV of $\hat{L}_3(t)$ because $X_*(t)$, which is an upstream signal, is not as noisy a signal compared to $\tilde{Z}_{X_*}(t)$. Lastly, the increase in bias in Step 3 can be traced to the use of both Auxiliary Results 2 and 3.

C Approximate product form distribution

The aim of this section is to show Auxiliary Result 2 in Appendix B, which states that, when the input is persistent, the joint probability distribution of the number of X_* and \tilde{Z}_{X_*} molecules is approximately given by the product a binomial distribution in X_* and a binomial distribution \tilde{Z}_{X_*} . The derivation makes use the framework of [14] to write two separate master equations, one for X_* and the other for \tilde{Z}_{X_*} .

Following the method of [14], we identify X_* as the fast variable which we will denote by x_f and \tilde{Z}_{X_*} as the slow variable denoted by x_s . We index the reactions (3a) to (3d) by $\ell = 1, 2, 3$ and 4. Let $a_\ell(x_s, x_f)$ be the propensity function for Reaction ℓ . Let also $s_{s\ell}$ and $s_{f\ell}$ be the stoichiometric coefficients for respectively, the slow and fast variables. From (3), we have:

$$\begin{aligned} a_1(x_s, x_f) &= k_+ a(M - x_f), & s_{s1} &= 0, & s_{f1} &= 1 \\ a_2(x_s, x_f) &= k_- x_f, & s_{s2} &= 0, & s_{f2} &= -1 \\ a_3(x_s, x_f) &= g_+ x_f (N - x_s), & s_{s3} &= 1, & s_{f3} &= -1 \\ a_4(x_s, x_f) &= g_- x_s, & s_{s4} &= -1, & s_{f4} &= 1 \end{aligned}$$

where a is the amplitude of the input signal and is assumed to be sufficiently high so that there is a high probability that x_f is far larger than N .

By assuming that the slow variable x_s rarely changes, [14] shows that the differential equation for the conditional probability $p(x_f|x_s)$ is given by:

$$\begin{aligned} p(x_s) \frac{dp(x_f|x_s)}{dt} &= \sum_{\ell=1}^4 (p(x_s - s_{s\ell}, x_f - s_{f\ell}) a_\ell(x_s - s_{s\ell}, x_f - s_{f\ell}) - \\ & p(x_s) p(x_f|x_s) a_\ell(x_s, x_f)). \end{aligned} \quad (53)$$

Although the RHS of (53) requires all 4 reactions to be accounted for, the effect of the slow reactions will be negligible. This assumption was used in [5]. We can justify this by the fact that if x_f is much larger than N , then the effect of the slow reactions on the fast variables will be small. After dropping the slow reactions from the RHS of (53) and by using the fact that $s_{s\ell} = 0$ for the fast reactions, we have:

$$\begin{aligned} p(x_s) \frac{dp(x_f|x_s)}{dt} &= \sum_{\ell=1}^2 (p(x_s, x_f - s_{f\ell}) a_\ell(x_s, x_f - s_{f\ell}) - \\ & p(x_s) p(x_f|x_s) a_\ell(x_s, x_f)). \end{aligned} \quad (54)$$

After cancelling $p(x_s)$ on both sides of the above equation, we have:

$$\begin{aligned} \frac{dp(x_f|x_s)}{dt} &= \sum_{\ell=1}^2 (p(x_f - s_{f\ell}|x_s) a_\ell(x_s, x_f - s_{f\ell}) - \\ & p(x_f|x_s) a_\ell(x_s, x_f)). \end{aligned} \quad (55)$$

Since both $a_1(x_s, x_f)$ and $a_2(x_s, x_f)$ are independent of x_s , this means $p(x_f|x_s)$ is independent of x_s . Furthermore, by using the forms of $a_1(x_s, x_f)$ and $a_2(x_s, x_f)$, we can show that at steady state $p(x_f|x_s)$ is given by the binomial distribution $B(X_*; M, k_+ a)$.

By using [14], we can show that the differential equation for $p(x_s)$ is given by:

$$\frac{dp(x_s)}{dt} = \sum_{\ell=3}^4 (p(x_s - s_{s\ell})\bar{a}_\ell(x_s - s_{f\ell}) - p(x_s)\bar{a}_\ell(x_s)). \quad (56)$$

where

$$\bar{a}_\ell(x_s) = \sum_{x_f} a_\ell(x_s, x_f)p(x_f|x_s). \quad (57)$$

By using the form of $a_3(x_s, x_f)$ and $a_4(x_s, x_f)$, as well as the fact that $p(x_f|x_s) \approx p(x_f)$, we have:

$$\bar{a}_3(x_s) = g_+ E[x_f](N - x_s) \quad (58)$$

$$\bar{a}_4(x_s) = g_- x_s \quad (59)$$

Furthermore, by using the forms of $\bar{a}_3(x_s)$ and $\bar{a}_4(x_s)$, we can show that at steady state $p(x_s)$ is given by the binomial distribution $B(\tilde{Z}_{X^*}; N, g_+ X_a)$. The result on the joint probability distribution $p(x_s, x_f)$ then follows from the above results.

D Utility maximisation

In this section, we will show that the utility maximisation problem (15) leads to a detection criterion based on likelihood ratio. The proof here uses the same method as Appendix 3A in [16] for proving the Neyman-Pearson lemma.

By using Lagrangian multiplier $\lambda \geq 0$, we rewrite (15) as the maximisation of:

$$P_{TP}P_1U_1 - \lambda(P_{FP}P_0C_1 + P_{TP}P_1C_1 - C_{\max}) \quad (60)$$

$$= (U_1 - \lambda C_1)P_1P_{TP} - \lambda C_1P_0P_{FP} + \lambda C_{\max} \quad (61)$$

Let \mathcal{O} be the observations that are available to the detection problem. Also let \mathcal{A}_0 and \mathcal{A}_1 be two disjoint sets which are to be used as the decision regions for the detection problem. In particular, the detection problem will decide for hypothesis \mathcal{H}_1 (resp. \mathcal{H}_0) if $\mathcal{O} \in \mathcal{A}_1$ ($\mathcal{O} \in \mathcal{H}_0$). Given these definitions, we can write P_{TP} and P_{FP} as:

$$P_{TP} = \int_{\mathcal{O} \in \mathcal{A}_1} P[\mathcal{O}|\mathcal{H}_1] d\mathcal{O} \quad (62)$$

$$P_{FP} = \int_{\mathcal{O} \in \mathcal{A}_1} P[\mathcal{O}|\mathcal{H}_0] d\mathcal{O} \quad (63)$$

By substituting (62) and (63) into (61), we have the objective to be maximised is:

$$\int_{\mathcal{O} \in \mathcal{A}_1} (U_1 - \lambda C_1)P_1 P[\mathcal{O}|\mathcal{H}_1] - \lambda C_1P_0 P[\mathcal{O}|\mathcal{H}_0] d\mathcal{O} + \lambda C_{\max} \quad (64)$$

In order to maximise (64), we should include \mathcal{O} in \mathcal{A}_1 if the integrand in (64) is positive. In other words, \mathcal{A}_1 should be the set of all \mathcal{O} 's such that:

$$(U_1 - \lambda C_1)P_1 \text{P}[\mathcal{O}|\mathcal{H}_1] - \lambda C_1 P_0 \text{P}[\mathcal{O}|\mathcal{H}_0] > 0 \quad (65)$$

If $U_1 - \lambda C_1 > 0$ then (65) is equivalent to:

$$\frac{\text{P}[\mathcal{O}|\mathcal{H}_1]}{\text{P}[\mathcal{O}|\mathcal{H}_0]} > \frac{\lambda C_1 P_0}{(U_1 - \lambda C_1)P_1} \quad (66)$$

This shows that we can use a criterion based on the likelihood ratio to maximise the utility. Note that if the requirement $U_1 - \lambda C_1 > 0$ holds, then a non-empty \mathcal{A}_1 may be found because the benefit gained (or utility) from deciding for \mathcal{A}_1 outweighs the cost required. Otherwise, if $U_1 - \lambda C_1 \leq 0$, (65) suggests that \mathcal{A}_1 should be an empty set.

Note that (64) can be interpreted as the maximisation of P_{TP} subject to an upper bound on P_{FP} , which is the same class of optimisation formulation that the Neyman-Pearson lemma considers.

We remark that we can see from the above derivation that if both the mean utility and mean cost are linear in the probabilities P_{TP} , P_{FP} , P_{TN} and P_{FN} , then the utility maximisation problem can be solved by using a criterion based on the likelihood ratio. We further remark that it is straightforward to generalise the above proof to the case with non-zero utility and cost.

E Necessity of delay

We use the method of contradiction to argue that there must be a delay in the cloud if $d_0 > t_{ss}$. Let us assume that there is a ‘‘memoryless’’ function $\psi(\text{E}[X_*(t)])$ which can carry out the computation in the cloud, i.e.

$$\psi(\text{E}[X_*(t)]) = g_- \pi(t) [\phi(\text{E}[X_*(t)])]_+ \quad (67)$$

Since we assume that the pathway (3) reaches the steady state by d_0 , we can find time instants t_1 and t_2 where $t_{ss} \leq t_1 < d_0 < t_2 < d$ such that $\text{E}[X_*(t)]$ is at steady state at both times t_1 and t_2 , i.e. $\text{E}[X_*(t_1)] = \text{E}[X_*(t_2)]$. Let us consider (67) at time instants t_1 and t_2 , we have:

$$\psi(\text{E}[X_*(t_1)]) = 0 \quad (\text{because } \pi(t_1) = 0) \quad (68)$$

$$\psi(\text{E}[X_*(t_2)]) = g_- [\phi(\text{E}[X_{*,ss}])]_+ > 0 \quad (69)$$

which is a contradiction because $\text{E}[X_*(t_1)] = \text{E}[X_*(t_2)]$. This establishes that, if $d_0 > t_{ss}$, there must be a delay in the cloud in Fig. 6.